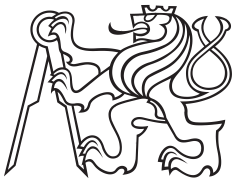

Czech Technical University in Prague

F3

Faculty of Electrical Engineering
Department of Electromagnetic field

Illuminating Optical Fiber Based Optical Camera Communications

Bc. Klára Eöllősová

Supervisor: Ing. Matěj Komanec, Ph.D.
Supervisor–specialist: MSc. Shivani Rajendra Teli, Ph.D.
Field of study: Electronics and Communications
Subfield: Photonics
January 2022

ZADÁNÍ DIPLOMOVÉ PRÁCE

I. OSOBNÍ A STUDIJNÍ ÚDAJE

Příjmení: **Eöllősová** Jméno: **Klára** Osobní číslo: **465353**

Fakulta/ústav: **Fakulta elektrotechnická**

Zadávající katedra/ústav: **Katedra elektromagnetického pole**

Studijní program: **Elektronika a komunikace**

Specializace: **Fotonika**

II. ÚDAJE K DIPLOMOVÉ PRÁCI

Název diplomové práce:

Illuminating optical fiber based optical camera communications

Název diplomové práce anglicky:

Illuminating Optical Fiber Based Optical Camera Communications

Pokyny pro vypracování:

The diploma thesis will focus on novel visible light communication principle using light emitting diode (LED) or laser coupled illuminating optical fibers (OFs) as a transmitter (Tx) and conventional optical cameras as a receiver (Rx).
The thesis will cover the theoretical background, analysis of the optical communication systems, a proposal of the measurement configuration and experimental validation of the proposed approach.
The student will carry out following tasks:
1) Study the state of the art in optical camera communications (OCC) and illuminating OFs. First, the focus will be on camera image capturing principles and camera design. Second, the focus will be on illuminating OFs, both from polymer and glass materials.
2) Analyze the illuminating OF based OCC (OF-OCC) system in terms of channel characteristics, bandwidth and data speed limitations, and effect of environmental noise such as ambient light, etc.
3) Analyze various sources (LEDs and lasers of different size, radiation pattern, illumination) with various illuminating optical fibers (silica and polymer, various core diameters) to find optimal coupling/excitation conditions for effective OF-OCC system.
4) Propose an OF-OCC measurement configuration based on points 2) and 3).
5) Experimentally characterize and demonstrate the proposed OF-OCC system, with respect to illumination, modulation frequency, fiber-to-camera distance, illuminating fiber shape, etc. Compare using LEDs vs. laser excitation and using various illuminating fibers.
6) Conclude on the overall OF-OCC system performance, its advantages and limitations and discuss possible future outlook.

Seznam doporučené literatury:

[1] Z. Ghassemlooy, L. Nero Alves, S. Zvanovec and M. Ali Khalighi, Visible Light Communications: Theory and Applications, CRC Press, 2017.
[2] Z. Ghassemlooy, P. Luo, S. Zvanovec, Optical Camera Communications, chapter in Optical Wireless Communications - An Emerging Technology, ed. M. Uysal et al., Springler, pp. 447-568, Springer, 2016.

Jméno a pracoviště vedoucí(ho) diplomové práce:

Ing. Matěj Komanec, Ph.D., katedra elektromagnetického pole FEL

Jméno a pracoviště druhé(ho) vedoucí(ho) nebo konzultanta(ky) diplomové práce:

Ing. Shivani Rajendra Teli, katedra elektromagnetického pole FEL

Datum zadání diplomové práce: **25.05.2021** Termín odevzdání diplomové práce: _____

Platnost zadání diplomové práce: **19.02.2023**

Ing. Matěj Komanec, Ph.D. podpis vedoucí(ho) práce	podpis vedoucí(ho) ústavu/katedry	prof. Mgr. Petr Páta, Ph.D. podpis děkana(ky)

III. PŘEVZETÍ ZADÁNÍ

Diplomantka bere na vědomí, že je povinna vypracovat diplomovou práci samostatně, bez cizí pomoci, s výjimkou poskytnutých konzultací. Seznam použité literatury, jiných pramenů a jmen konzultantů je třeba uvést v diplomové práci.

. _____ _____

Datum převzetí zadání Podpis studentky

Acknowledgements

I would like to thank my supervisor Ing. Matěj Komanec, Ph.D., for my thesis's overall guidance and coordination, for all the time and advice given when writing this thesis. Special thanks go to my supervisor-specialist Shivani Rajendra Teli, Ph.D., for introducing the basics of optical camera communications to me and for her invaluable advice, and to prof. Ing. Stanislav Zvánovec, Ph.D., for highly helpful comments on my thesis. Next, I would like to thank Ing. Vojtěch Neuman for technical support with TikZ and MATLAB. Also, I would like to thank SQS for providing material for the measurements.

Last, I would like to thank my family and friends for everything they have ever done for me, for all the support, encouragement, time, and patience. Finally, I would like to thank my fiancé Jirka for always being there for me, never letting me down, and motivating me to be the best I can be.

Declaration

I declare that I have written submitted thesis by myself and that I have listed all information sources in accordance with Methodical Guideline on Compliance with Ethical Principles.

Prohlašuji, že jsem předloženou práci vypracovala samostatně a že jsem uvedla veškeré použité informační zdroje v souladu s Metodickým pokynem o dodržování etických principu při přípravě vysokoškolských závěrečných prací.

Abstract

This thesis presents a novel concept of optical fiber-based optical camera communication (OF-OCC). Based on the characterization of selected light sources and illuminating optical fibers, I propose their optimal combination for OF-OCC in the framework of optical wireless communication. Afterward, I present OF-OCC measurement scenario, which is subsequently assembled, characterized, and evaluated. The key experimental result suggests that such an OF-OCC system can work reliable up to 3 m distance with a modulation frequency of 300 Hz. Finally, I conclude with future outlook and possible OF-OCC system enhancements.

Keywords: Optical Camera Communication, Illuminating Optical Fiber, Light-Diffusing Fiber, Side-Emitting Fiber, Plastic Optical Fiber, Optical Wireless Communication

Supervisor: Ing. Matěj Komanec, Ph.D.
Fakulta elektrotechnická,
Technická 2,
16000 Praha 6,
B2-533

Abstrakt

V této práci představuji nový koncept komunikace pomocí optické kamery založené na optických vláknech (OF-OCC). Na základě charakterizace vybraných zdrojů světla a osvětlovacích optických vláken navrhuji jejich optimální kombinaci pro OF-OCC v rámci optické bezdrátové komunikace. Dále se zaměřím na konfiguraci měření OF-OCC, který následně sestavím, charakterizuji a vyhodnotím. Hlavním výsledkem experimentální části je, že takovýto OF-OCC systém může spolehlivě fungovat až do vzdálenosti 3 m s modulační frekvencí 300 Hz. Na závěr uvádím budoucí směry vývoje, možné varianty OF-OCC systému a jeho vylepšení.

Klíčová slova: komunikace pomocí kamery, vyzařující vlákno, stranově vyzařující vlákno, plastové optické vlákno, optická bezdrátová komunikace

Překlad názvu: Komunikace kamerou založená na vyzařujícím optickém vláknu

Contents

Figures

Tables

List of Acronyms

Acronym	Meaning
ADC	Analog-to-Digital Converter
APD	Avalanche Photodiode
AWG	Arbitrary Waveform Generator
BT	Bias-Tee
BER	Bit Error Rate
CMOS	Complementary Metal–Oxide–Semiconductor
CSK	Color Shift Keying
CW	Cold White
DL	Diffusion Length
EM	Electromagnetic
GS	Global Shutter
FOV	Field-of-View
FSO	Free Space Optics
FWHM	Full Width at Half Maximum
IM	Intensity Modulation
IOF	Illuminating Optical Fiber
IR	Infrared
IS	Imaging Sensor
LCD	Liquid Crystal Display
LD	Laser Diode
LDF	Light-Diffusing Fibers
LED	Light-Emitting Diode
MFTP	Maximum Flickering Time Period
MIMO	Multiple-Input Multiple-Output
MSE	Mean Square Error
NA	Numerical Aperture
NIR	Near Infrared
NRZ	Non-Return-to-Zero
OCC	Optical Camera Communication
OFDM	Orthogonal Frequency Division Modulation
OF-OCC	Optical Fiber based OCC
OOK	On-Off Keying
OWC	Optical Wireless Communication
PD	photodiode
PM	Pulse Modulation
PMMA	Polymethyl Methacrylate
POF	Plastic Optical Fiber
PSNR	Peak Signal-to-Noise Ratio
ROI	Region-of-Interest
RGB	Red-Green-Blue
RS	Rolling Shutter
Rx	Receiver

Acronym	**Meaning**
SB	Super Bright
SG	Side Glow
SI	Step Index
SNR	Signal-to-Noise Ratio
Tx	Transmitter
UV	Ultra Violet
VLC	Visible Light Communication
VIS	Visible Light
WW	Warm White

List of Notations

Symbol	Meaning
α	Attenuation Coefficient of an Optical Fiber
η	Quantum Efficiency of an IS
θ	Angle of Rotation of a Rx
λ	Wavelength
Φ	Luminous Flux
d	Rx-IOF Distance
d_{cladding}	Cladding Diameter of an Optical Fiber
d_{core}	Core Diameter of an Optical Fiber
d_f	Size of a Captured IOF Part
d_{max}	Rx-IOF Distance - maximum
d_{min}	Rx-IOF Distance - minimum
E_e	Flux Density of a Light Source
f_c	Focal Length of a Camera
f_R	Frame Rate
f_s	Modulation Frequency
G_V	Gain
$h(t)$	Impulse Response of a Channel and a Camera
I	Current
I_F	Forward Current
L	Illumination
l	Length of the Fiber
l_{IS}	Size of an Image Sensor
l_{Tx}	Size of a Transmitter
n	Refractive Index
$n(t)$	Noise
n_{cladding}	Refractive Index of a Fiber Cladding
n_{core}	Refractive Index of a Fiber Core
$t_{\text{row-exp}}$	Exposure Time of One Row
$t_{\text{row-shift}}$	Time Delay Between Rows
N_{groups}	Number of Data Transmission Channels in a Tx
N_{row}	Number of Pixel Rows of a OCC System
N_{visible}	Number of Visible Bits per Group
$P(0)$	Illuminating Power of a Light Source
$P(z)$	Illuminating Power of an Optical Fiber
R_b	Data Rate
R_{IOF}	IOF Bend Radius
R_{packet}	Packet Rate
s	Bit Sequence of One Packet
t_F	Exposure time
t_{frame}	Time Frame of a Rx
V_{RF}	Modulation Voltage
V_s	Supply Voltage

Symbol	**Meaning**
V	Voltage
V_{ADC}	Voltage of a ADC
V_{pixels}	Voltage of a Pixel
$x(t)$	Transmitted Intensity-Modulated Light
$y(t)$	Received Signal
z	Distance from a Light Source

Chapter 1

Introduction

In today's modern world, we are surrounded by the omnipresent information flow - from the Internet as we know it, through vehicle-to-vehicle (V2V) communication, Industry 4.0, various sensors, all being a part of the upcoming Internet of Things (IoT). The need for flexible and secure data transfer is continuously growing, thus creating a need for new technologies and data transfer schemes. For decades, conventional optical fibers have had a key role in high-speed data transfer. However, illuminating optical fibers (IOFs) present an unexplored area of research, especially in sensory networks in the framework of IoT.

This thesis introduces a novel concept of an optical wireless communication system based on an optical camera and an IOF coupled with a light source. Once the light source is coupled to the IOF, simultaneous illumination and data transfer can be realized.

The IOF could be placed, e.g., around a door, and according to the current situation inside the room (for example, "on-air"), the data in the fiber could inform the newcomer about the situation by simple scanning the IOF with a mobile phone camera using optical camera communication (OCC). Before the technology is developed to this level of user-friendly application, it is necessary to study the fundamental aspects of the IOF-based OCC system.

This thesis presents the theoretical background for IOF camera communication channels: characterization measurements of light sources and IOFs and presents experiments of IOF-based OCC. First, the theoretical background is presented. The principle of optical wireless communication is defined with an emphasis on OCC. Following, the IOFs are discussed, several applications of this type of fibers are proposed and the main differences between silica, and plastic IOFs are described.

Second, initial experimental measurements are presented. In order to decide the optimal light source and IOF combination, it was necessary to perform several measurements. As IOF, silica and plastic optical fibers were considered. Based on radiation pattern and illumination performance, the plastic IOFs were chosen for further experiments. As for light sources, an LED and a laser were considered.

Next, the IOF-based OCC measurement is presented. The proposed experimental scheme provides a cost-effective approach and can be used to

transmit basic information such as sensoric data, localization data, safety data within indoor IoT environments, and also small identification information. The quality matrices of the captured data with respect to camera gain and exposure time and data modulation frequencies are analyzed in terms of the success of reception of received data.

Chapter 2

Optical Wireless Communication

Optical communication systems can be divided into two main groups [1]: fiber-optic communications and optical wireless communications (OWC). OWC can be further divided into two categories [2]: free-space optics (FSO) and visible light communication (VLC) with subcategory of optical camera communication (OCC). Comparison of FSO, VLC and OCC is presented in Table 2.1.

In OWC [1], the receiver is usually a non-imaging device, such as a PIN photodiode (PD) or an avalanche photodiode (APD). Photodiodes generally work in a linear regime according to the incident light power. However, PDs are fairly small ($\sim$ mm^2) in comparison to the transmission distance (in the order of meters to hundreds of meters). Therefore at longer distances, the detected signal power is reduced due to the small PD area, which leads to lower signal-to-noise (SNR) and thus limits the transmission range. A concentrator may be used in front of PD to increase the received optical power and thus improve data rate (marked as R_b) [1]. On the other hand, transmission distance is then shortened and it is more difficult to separate the optical signals, as well as the mobility is worsened. Mobility is the ability of the transmitter–receiver pair to move around and yet to preserve its wireless functionality [3]. Thus if the receiver has to be close to the transmitter, the device can not move far away and the mobility is going to worsen.

Table 2.1: Comparison of OWC categories.

	Transmitter	Reciever	Spectrum	Limitations
FSO	laser	PD/APD	IR/VIS/UV*	sensitive to weather and turbulence
VLC	LED/LD*	PD/APD/ /PIN/camera	IR/VIS*	illumination constraints, limited range, vulnerable to mobility
OCC	LED/screen	camera	IR/VIS	low data rate

**Laser Diode (LD), Infrared (IR), Visible Light (VIS), Ultra Violet (UV)*

OWC is widely used in the car industry, where cameras are also used for sensory applications. Cameras inside the car can monitor driver's attention, PDs can detect luminosity levels and based on the measured data they can

e.g., automatically switch on and off the headlamps. Cameras outside the car can watch for blind spots, read road signs, etc. Sensors can also detect other vehicles and monitor distance and lane departure. Infrared (IR) light-emitting diodes (LEDs) and PDs are used to detect rain and automatically activate wipers [1].

FSO could be used to achieve long transmission distances together with ultra-high data rated (according to [4] 100 Gb/s over 10 km distance, 1 Tb/s over 4 km distance) while still having flexible coverage, thanks to beamforming techniques. However, FSO can be easily blocked by physical barriers and is sensitive to link conditions such as atmospheric turbulence or fog, which can significantly affect the performance of the link [2].

2.1 Visible Light Communication (VLC)

In VLC, off-the-shelf LEDs are used to simultaneously offer communication channel as well as regular lighting. Transmission rate of such a VLC channel can be up to several Gbps [5]. VLC is usually designed in multiple-input multiple-output (MIMO) settings. Receiver in VLC can be an image sensor (or a camera in OCC) consisting of a PD array and a built-in readout circuit. The amount of electrons generated in each pixel of the image sensor is proportional to the received optical spectral density together with responsivity of a pixel. As the image sensor is a two-dimensional PD array consisting of more than 10 million pixels, the spatial resolution is very high. Therefore, spatial-division multiplexing and imaging MIMO systems can be used in VLC, since the camera can separate light from different directions. An example of VLC communication is shown in Fig. 2.1. Possible modulation schemes according to [2] are Orthogonal Frequency Division Modulation (OFDM), On-Off Keying (OOK), Intensity Modulation (IM), Pulse Modulation (PM), Color Shift Keying (CSK), and others.

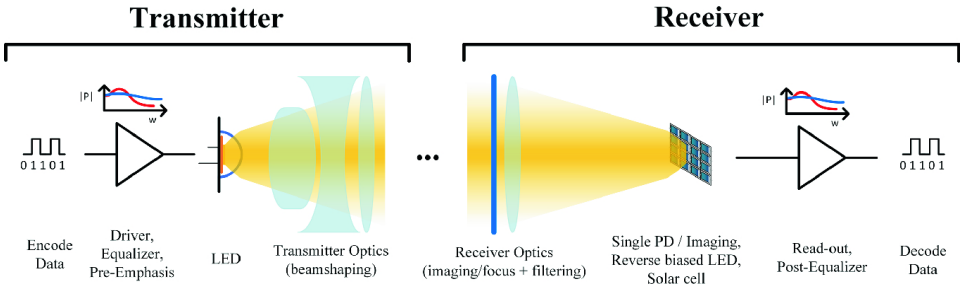

Figure 2.1: An example of Visible Light Communication [6].

Despite VLC's several inherent limitations (e.g., the path loss dramatically increases with distance, hence restricting long-range communication), it is still a very promising technology. It is a safe and secure directional communication with a wide range of applications: indoor high-speed internet access, information downloading, indoor positioning, underwater OWC for autonomous underwater vehicles (underwater VLC), car-to-car/vehicle-to-

vehicle communication, communication using street lighting, and outdoor vehicular to infrastructure networking [7].

2.2 Optical Camera Communication (OCC)

Optical camera communication (sometimes also denoted as camera-based VLC) [5], is a system consisting of a transmitter - an LED, a display, or a digital sign - and a receiver: a camera sensor of a digital camera, a smartphone camera, an industrial camera, or a webcam [7]. OCC is based on the knowledge from VLC while embedding a camera without modifying the hardware. The fact that smart devices in our daily lives are equipped with cameras is one of the main motivations for OCC [2]. OCC offers low cost, spatial and wavelength separation ability, larger receiver field-of-view (FOV) and other unique features. OCC is described in the IEEE standard work group 802.15.7m [8], which consist of the revision of a VLC standard to incorporate OCC functionalities and modifications.

2.2.1 Receivers

Cameras used as receivers in OCC consist of an imaging lens, an imaging sensor (IS) and other supporting components [1]. The digital IS is usually a two-dimensional array of PDs. In most smartphones, a complementary metal–oxide–semiconductor (CMOS) technology-based active pixel sensors are used. The same detector is usually also used in VLC for lower bit rate R_b.

A color filter array (see Fig. 2.2) is placed above an image sensor array to obtain the color information. The filter can be either Bayer color filter array with green (G), red (R) and blue (B) pixels, where the number of

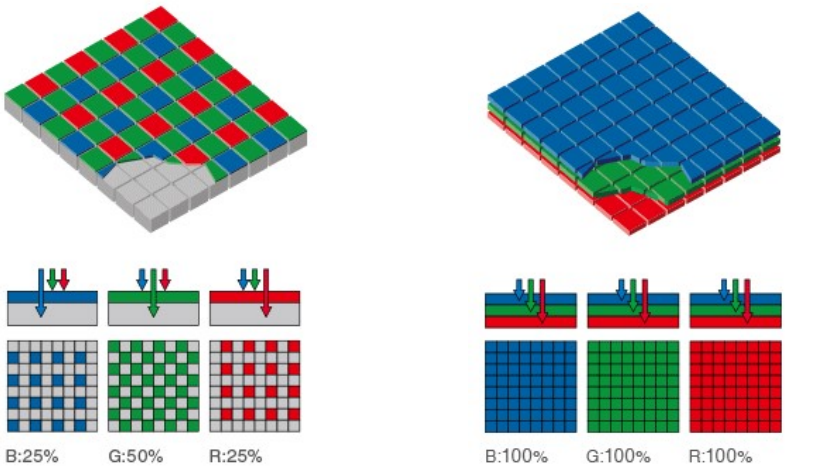

(a) : The Bayer Filter Image Sensor. **(b) :** The Foveon X3 Image Sensor.

Figure 2.2: Types of color filters of an image sensor [9].

green pixels is the same as number of red and blue pixels combined. This is due to the wavelength-dependent sensitivity of human eye. Furthermore, by adding redundancy to green pixels, less noisy image and finer details can be achieved compared to filter with equal number of each color. By using the color array the RGB signal is separated. Alternatively, a Foveon X3 pattern-based color filter array can be used instead of Bayer pattern [2]. The advantage of the Foveon X3 array is that it enables to capture 100 % of the RGB color information, whereas Bayer filter is covered only from 50 % by green sensitive cells and mere 25 % each blue and red cells [9]. For comparison see Fig. 2.2.

2.2.2 OCC Signal Detection

It is possible to achieve higher data rate R_b by using MIMO technique: multiple LEDs as transmitters combined with a single camera as a receiver. Since each pixel of the camera is in fact an independent PD, it is possible to separate light coming from different directions [1]. There are two options with MIMO technique: imaging and non-imaging MIMO system (this system can be used in VLC systems in general). The imaging MIMO has an IS and an imaging lens, which are used to separate different light signals. This option offers multiple access and increases R_b, improves signal-to-noise ratio (SNR) and reduces the bit error rate (BER). The non-imaging MIMO VLC system uses a receiver with a non-imaging lens with multiple PD, where light signals from all LEDs are received by each PD. One advantage of non-imaging MIMO is that lenses used in imaging MIMO usually have a small FOV, so mobility limits are better using non-imaging MIMO compared to imaging MIMO.

A conventional camera has typically low frame rates (i.e., 20-50 fps), which leads to light flickering [1]. Therefore if a transmitter is using visible light and the signal frequency is below the maximum flickering time period (MFTP) of human eye (around 200 Hz) the flickering is detectable by human eye [10].

This can be solved using one of two options. First, an under-sampled modulation scheme can be applied so that the data rate is increased, e.g. on-off keying modulation (OOK). Or second, through a specific method of capturing a still picture or video frame - rolling shutter (RS) or global shutter (GS) of CMOS camera [1]. For comparison see picture 2.3.

GS exposes all pixels of the image sensor at one time, so the entire picture or the video frame is captured simultaneously. Whereas RS captures light from an image sensor in a row-by-row process. Only one row of the sensor being exposed at the time [1]. The shutter is not physically moving across each row of pixels horizontally or vertically. But when the row of the digital rolling shutter camera's sensor is supposed to be exposed, the camera tells the row to become light-sensitive. A very fast clocking frequency is needed for this special row-by-row exposure, otherwise the time delay between each row may be significant. The light source is flickering at a lower frequency than RS is scanning with, but at higher frequency than MFTP of human eye [1].

By this method, the light signal is captured at a high frequency (few kHz) so the flickering is not visible by human eye. However, dark and bright strips can be captured by RS cameras.

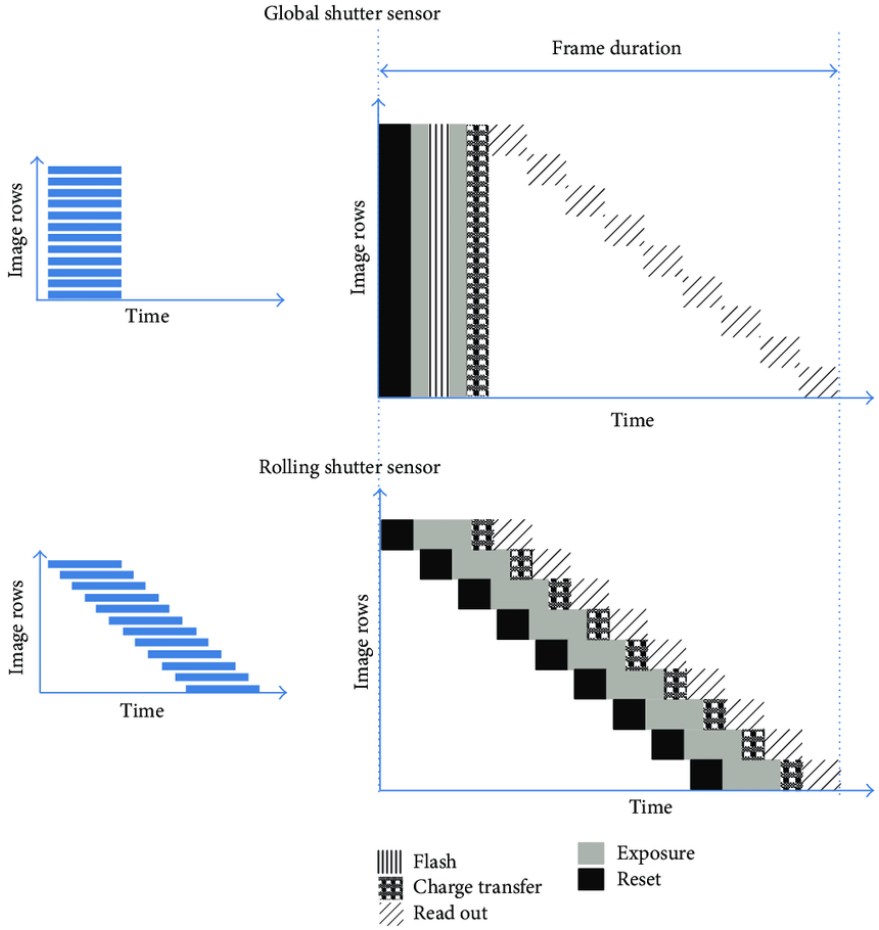

Figure 2.3: Principle of global shutter vs. rolling shutter camera capturing method [11].

OCC could be improved in several ways. It could be used in full-duplex settings, instead of simplex settings, for instant messaging or two-party interaction [2]. For now, the duplex settings are limited due to interference, which may occur. Another aspect, limiting OCC, is strong ambient radiation such as solar irradiance or street lamps, which leads to image sensor saturation. The communication data rate could be improved through modulation of frequency, phase, and intensity. Alternative options of ultra-high frame rate camera are still too pricey for widespread application. And since most commercial cameras have a lower frame rate (from 30 fps to several hundred fps) typical data rate is lower than several bit/s/pixel (bits per second per pixel) according to Nyquist sampling theorem, the maximum symbol rate is lower than 15 sps (symbols per second). Additionally, the low frame rate could be detected by human eyes, so it is not possible for LED transmitter to use such a low frequency to match the low frame rate of the sensor.

2.2.3 Application of OCC and Future Directions

Similarly to VLC, OCC has a wide range of applications [1]. From indoor positioning and navigation to vehicle-to-vehicle, vehicle-to-infrastructure and vehicle-to-pedestrian communication (which can be summarized as intelligent transportation system - ITS) [2]. Digital signage could be used to obtain information by scanning it with a smartphone for a secure data sharing and transformation. Since camera-based visible light systems are free of electromagnetic interference, compared to other RF-based systems, the positioning system offers not only high positioning accuracy, but it can be used in electromagnetic field-sensitive environment. Other applications may be posture and gesture detection and recognition. Or wearable sensors used for health data collection, that could be easily analysed by a camera-carrying robot. One of the main weaknesses of OCC is data rate. In some applications (e.g. remote controlling, vehicle steering, and indoor positioning and navigation) cost and accuracy may be the main restrictive factors.

Chapter 3

Illuminating Optical Fibers

The most common application of optical fibers is high-speed long-distance data transfer, where it is desirable to minimize fiber attenuation to transmit with minimal losses.

On the other hand, there are applications, such as lighting interior design, where a special type of optical fiber - an illuminating optical fiber (also called side-emitting fiber) - is used. To this special type of optical fibers, emitting light at multiple points or along the entire fiber length, the next Section is dedicated.

3.1 Principle of IOF

Illuminating optical fiber could be described as a linear lighting device designed to intentionally radiate the propagating light over its length and in all directions perpendicular to the direction of propagation [12]. IOFs can thus serve as distributed light sources. Since multimode fibers have number of higher modes which allow higher emission from fiber's surface, they are usually used for IOFs [13]. The diameter of the IOF core d_{core} ranges from 0.2 mm to even 30 mm and is thus many times greater than the wavelength of light propagation in the IOF [14]. In comparison to fibers with smaller diameter, the higher diameter IOFs have a higher illumination power [13].

As the technology of IOF is relatively new, the nomenclature is not yet fully unified. Therefore illuminating optical fibers can be found under other names such as side-emitting fibers or light diffusing fibers (LDFs).

The emission of light from the IOF's surface can be achieved by several methods. First [13], if the light source is launching light into the fiber at angles larger than the critical angle, the non-guided light escapes the fiber in form of side emission. This effect can be obtained by decreasing the refractive index of the fiber core n_{core}, by increasing the refractive index of the fiber cladding n_{cladding}, or by changing the angle of incident light. By changing the refractive indexes, the numerical aperture (NA) of the fiber would increase to values from 0.35 to 0.53 in silica IOFs in VIS spectrum [15]. The coupling to the fiber may be accommodated to be suitable for a variety of light sources, mainly for LEDs (Lambertian emitter) and laser diodes (narrow output beam). The radiant intensity of a Lambertian emitter is proportional to $\cos\theta$. This

is known as Lambert's law of intensity [16]

$$J_\theta = J_0 \cos\theta, \tag{3.1}$$

where J_θ is the intensity of a small incremental area of the source in a direction at an angle θ from the normal to the surface, and J_0 is the intensity of that incremental area in the direction of the normal. This means that the radiance of a Lambertian emitter is constant with respect to θ.

Second, the material of the fiber can be modified to deliberately scatter the propagating light. According to [13], it is possible to use micro-bending of the core or the cladding, mix fluorescent or scattering additives in the fiber material. By this a geometric asymmetry in the core/cladding is created, causing reflection or fluorescence into core/cladding. By creating these scattering centers in the fiber core, very efficient scattering of the light through the sides of the optical fiber is provided [15]. As stated in [12] this effect can also be achieved by adding scatterers (impurities), impairing the refractive indices of the core-cladding interface, etching gratings, or introducing fluorescent additives. In Fig. 3.1, a comparison of the cross-section of an end-emitting fiber and side-emitting fiber (i.e., IOF) with indicated scattering centers is demonstrated.

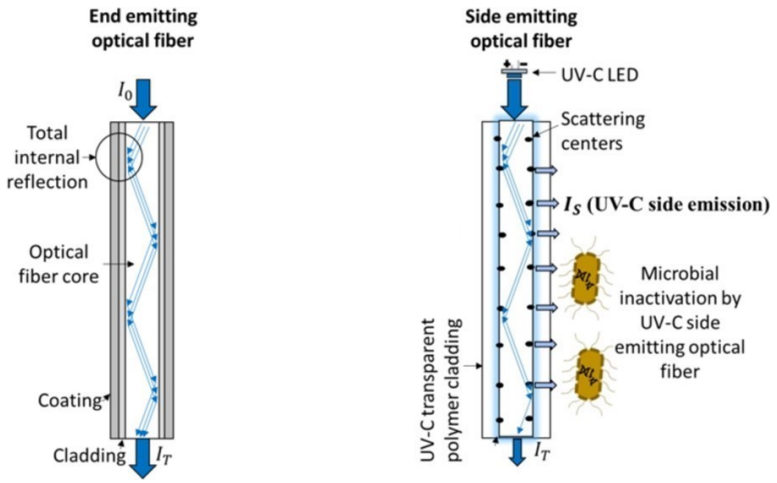

(a) : End-emitting fiber. **(b) :** Side-emitting fiber / IOF.

Figure 3.1: Cross-section of an end-emitting fiber and a side-emitting IOF [17] showing medical application for inactivation of microbes by UV-C light.

The luminous flux Φ_e emitted by the IOF depends on the given flux density of the light source E_e, the core diameter of the IOF d_{core}, attenuation of the IOF α and distance from the light source l [13]. As anticipated, with increasing distance l from the light source, the intensity of radiation emitted by the IOF decays. The percentage of light emitted per unit of length is constant over the entire IOF length. With distance, the emitted energy diminishes exponentially. In Fig. 3.2, the differential element of IOF is depicted. The

optical intensity at any point in the fiber $I(l)$ can be determined [12] by:

$$I(l) - (I(l) + \frac{\partial I(l)}{\partial l}\mathrm{d}l) = \gamma I(l)\mathrm{d}l, \tag{3.2}$$

where γ is the loss coefficient due to side emission. The emitted optical intensity at any point of the fiber $I_s(l)$ can be computed [12] by:

$$I_s(l) = \gamma \frac{I_0}{4\pi} e^{-\gamma l}, \tag{3.3}$$

where the initial optical intensity is set to I_0. This equation represents a simplified model of IOF.

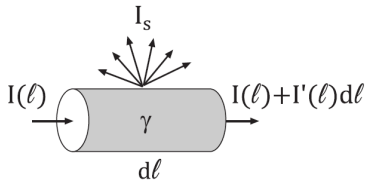

Figure 3.2: Differential element of an IOF [12].

The decrease of the illuminating power $P(l)$ (power illuminating from the fiber surface) of the fiber at a given place can be determined [13] with equation

$$P(l) = P(0)10^{-\alpha l/10}, \tag{3.4}$$

where $P(0)$ is the illuminating power of the light source, α is the attenuation coefficient of the optical fiber and l is the distance from the light source. The attenuation coefficient α illustrates the attenuation value over the fiber length.

A high level of illumination loss (loss in illuminating power) could be due to fiber bending leading to light transmission into the cladding. The side emission is generally assumed to be much higher than extinction ($\gamma >> \alpha$), and that the radiation mechanism leads to an isotropic radiator.

As suggested in [13], there is a way to modify the efficiency of the side emission over the length of the fiber, if a uniform emitted intensity is required over the fiber length. An optical fiber with notches cut through cladding into the core could be used, see Fig. 3.3. By changing the distance between

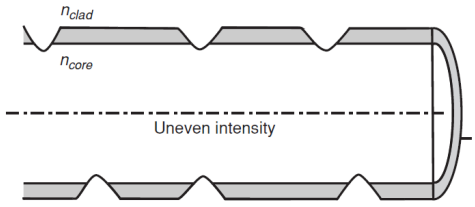

Figure 3.3: IOF with notches through cladding [13]. The notches ought to modify the efficiency of the side emission over the length of the IOF.

the notches according to the distance from the light source, emission of uniform intensity can be achieved over the fiber length. According to [12], fibers with a side emission coefficient depending on distance ($\gamma(l)$) are theoretically achievable, but their cost would be immense and thus would not be widely used.

3.2 Applications of IOFs

For certain applications, e.g., for illumination purposes, light emission along the fiber is needed. IOFs can be used to create optically active textile structures, to highlight people and objects without the need for external exposure [13], or simply for design purposes in clothing and indoor lighting. Other illuminating applications may include light decoration of water construction (fountains, pools), illumination of places endangered with explosions, illumination of museum exhibits [14]. By the use of phosphorous coatings the emitted light may also be converted to different colors.

Unique illumination application, see Fig. 3.4, can be achieved by coupling the fiber to flat glass to make a very low bezel illumination fixture - transparent glass with an IOF placed to the side of 0.7 mm glass. This setup is similar to back light unit used for liquid crystal displays. The glass would have a coating on the surface, so the coupled light would be scattered to the wave-guiding plate [15].

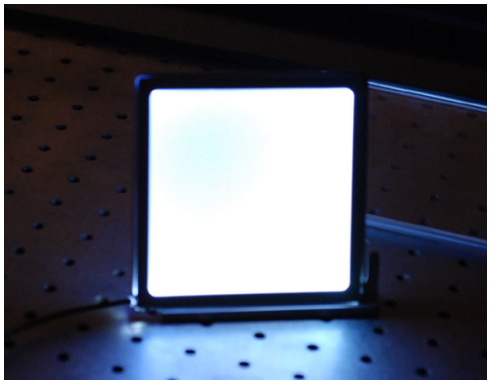

Figure 3.4: 4”x4” glass plate with scattering top layer with IOF coupled to the side of the plate [15].

In Fig. 3.1, another application of IOF was shown, this time for medical purposes. Ultra violet-C (UV-C) light is used as a light source, which is connected to an IOF and used for microbial inactivation in water [17]. Namely, Escherichia-coli can be prevented from growth or inactivated both on nutrient-rich surfaces and in water [17][18].

3.3 Advantages of IOFs

In optical wireless communications (OWC, see chapter 2), the use of IOFs could reduce the misalignment sensitivity due to their wider spatial distribution in comparison to traditional point-source-based OWC channels [12].

In special lighting applications, the flexibility of thin glass fibers enables the IOF to be set up in complex configurations and shapes. Furthermore, the light from the fiber can be coupled into glass sheets also for illumination purposes.

By placing yellow phosphor such as Ce-YAG (Cerium-doped Yttrium Aluminium Garnetused; for white LED) on the surface of the fiber, it is possible to create a flexible bright white light source. According to [15] the illumination of specific IOFs can exceed 10000 lux.

Another advantage of IOFs in lighting applications is that the IOF can be connected to low loss delivery fiber, which is connected to a remotely placed source. This brings additional flexibility to the lighting fixture designs and helps to deal with heat dissipation [15].

For IOFs, the diffusion length (DL) parameter can be defined [19]. The power emitted from the fiber decreases exponentially. The amount of power emitted from the fiber at its beginning is P_0 and one diffusion length is defined as IOF diffusion length at which the emitted power equals to $P_0/10$.

3.4 Silica IOFs

This Section focuses on silica-based IOFs developed by Corning under the brand name Fibrance® [19]. The outer diameter of the Fibrance is about 900 μm, from which $d_{\text{core}} = 170\,\mu$m is the glass core diameter, 60 μm is the thickness of the silica cladding, which is covered in polymer coating [19].

It is possible to place scattering materials in the coating to provide a fiber with a uniform angular scattering distribution. Fibrance has in its silica core a ring of non-periodically distributed (radially and axially) scattering centers. They range in size from $50-500$ nm in diameter, thus they effectively scatter the propagating light almost independently of the wavelength of light used [15].

Due to the large core diameter of the Fibrance core and numerical aperture (NA=0.5), low loss light coupling from inexpensive laser sources is possible. The sources can be visible or near infrared (NIR) laser diodes with efficiencies higher than 85%. Furthermore, fiber bundles with roughly 40 fibers can be created with coupling efficiency $\sim 50\%$ to LED sources [15]. The bending losses are small with minimum bending diameters as small as a 5 mm radius. The scattering losses can be as high as $5-7$ dB/m and the absorption losses within the fiber are negligible [15].

3.5 Plastic IOFs

Plastic (polymer) based IOFs are typically made of Polymethyl Methacrylate (PMMA) with refractive index $n = 1.49$ at $\lambda = 632\,\text{nm}$. [20] Fluoropolymers, with refractive index $n \sim 1.35$ to 1.43, are used as cladding polymers. Relation $n_{\text{core}} > n_{\text{cladding}}$ still applies [12][13].

Polymer materials are often chosen due to their cost efficiency and light-coupling capabilities. In comparison to silica glass IOFs, which usually have smaller core diameters and therefore tend to be more flexible, PMMA is very low-cost [13]. It is possible to make plastic optical fibers (POFs) with large d_{core}, which are easy to connect, but tend to be less flexible.

Plastic IOFs have a number of variations and a wide variety of applications. There are not only side-emitting fibers but also sparkle fiber optic cables that emit light from their sides on cuts in the fiber cladding. This type of IOF is especially interesting for design applications even in fashion industry.

Even traditional side-emitting fibers have more variations. For example, company ZDEA has either Super Bright solid core IOFs or Side Glow solid core IOFs [21]. The main difference is in different DL. The Super Bright IOFs a have much shorter DL (around 1 m), whereas the Side Glow IOFs have a DL of up to 10 m.

Chapter 4

Characterization of Light Sources and IOFs for OF-OCC

In this Section I present experimental results from performance characterization of selected light sources and IOFs for OCC with the result of an optimal combination of IOF and a light source. To achieve this goal, I characterized radiation patterns, illumination of both IOFs and light sources, and captured transmission spectra of selected IOFs.

4.1 Experimental Setup

The majority of the measurement discussed in this thesis is based on a variation of a fundamental light source-IOF setup, which is shown in Fig. 4.1. The input end of the IOF is attached to a 5D stage (3D + pitch and yaw), by using this stage, the IOF was placed as close to the light source as possible. The 5D stage was then used to maximize the coupling efficiency from the light source into the IOF. The 1 m-long IOF was attached horizontally and at the output end of the fiber a power meter (PM) or an optical spectrum analyser (OSA) was placed. A photo of the setup is shown in Fig. 4.2.

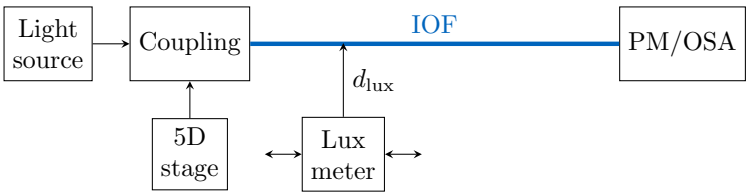

Figure 4.1: Characterization setup of IOF measurements with LED or laser diode as a light source. PM - power meter, OSA - optical spectrum analyser. To the side of the IOF, a lux meter is moved alongside to capture illumination levels at a distance d_{lux}.

In table 4.1 used devices for the initial measurements are listed. A lux meter, a power meter and spectrometer were used for illumination measurements, signal analysis and IOF transmission spectra analysis, respectively.

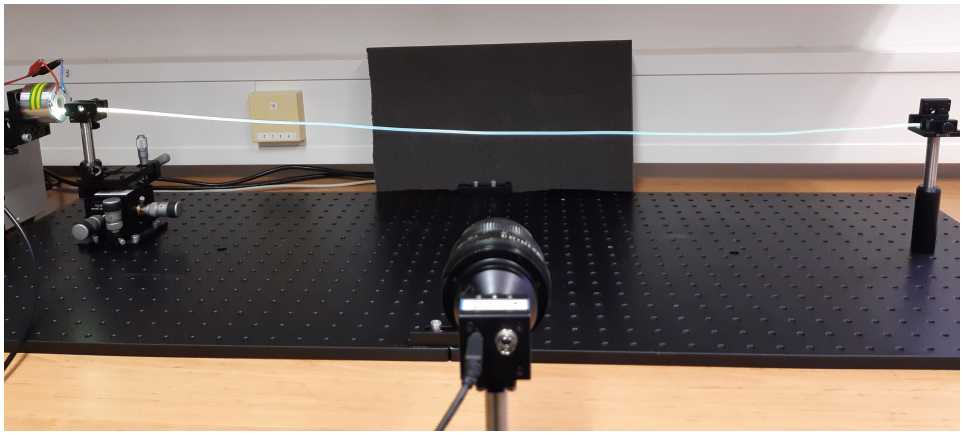

Figure 4.2: Measurement configuration for IOF's illumination analysis - horizontally attached IOF with LED light source. In the foreground (facing the IOF) a camera is placed.

Table 4.1: An overview of the used devices for IOFs characterization.

Device	Specifications
Lux meter	Voltcraft, MS-200LED, ±3 % accuracy
Power meter	Thorlabs, S121C, wavelengths 400-1100 nm
Spectrometer	Ocean Insight, Flame-S, VIS-NIR (350-1000 nm)
DC power supply	GW Instek, GPD-4303S

For alignment I used the following mechanical components:

- 5D stage - 3D micromovement stage Thorlabs (MAX313D/M) with pitch and yaw tilt platform Thorlabs (APY002/M)
- rotation stage - two-Axis Linear Translation Stage with Rotating Platform Thorlabs (XYR1)

4.2 Characterization of Light Sources

In order to characterize the light sources, I used measurement techniques described in this Section. The characteristics of the light sources are also presented in this Section.

4.2.1 List of Light Sources

All light sources, LEDs and a red laser diode (LD), are listed in table 4.2. The LEDs were cold white (CW) and warm white (WW) LEDs by Light Avenue with size of $\sim 500 \times 500\,\mu$m (LA CW20WP6 and LA WW20WP6) and $\sim 700 \times 700\,\mu$m (LA CW28WP6). The LA WW20WP6 was used mainly for examination of changes of color in plastic IOF, which is described in the next Section - 4.3.5. Typical luminous flux is Φ =55 lm at forward current of I_F =175 mA and Φ = 110 lm at forward current of I_F =350 mA, respectively. One set of $500 \times 500\,\mu$m LA CW20WP6 LEDs was complemented with an embedded lens with divergence of 10°. Fig. A.1 shows photos of all measured LEDs. Since for this thesis originally only the $500 \times 500\,\mu$m

LA CW20WP6 LEDs were available; therefore, the initial measurements were carried out with this LED.

The LD was Thorlabs' L635P5 LD (635 nm, 5 mW) which was attached on a laser diode mount (Thorlabs, LDM9T/M with integrated temperature controller). This mount includes a high bandwidth bias-tee circuit that allows RF modulated signals to be added to the laser controller signal. The beam divergence (full width at half maximum/ FWHM) of output power of 5 mW is 8° for parallel beam and 32° for perpendicular beam. For spectral measurements, a halogen light source (HL-2000-FHSA, max 4.5 mW, 360 – 2400 nm) by Ocean Insight was used.

Table 4.2: An overview of the used light sources.

Name	Type	Manufacturer	Size
CW28WP6	cold white LED	Light Avenue	$700 \times 700\,\mu$m
CW20WP6	cold white LED	Light Avenue	$500 \times 500\,\mu$m
CW20WP6+lens	cold white LED	Light Avenue	$500 \times 500\,\mu$m
WW20WP6	warm white LED	Light Avenue	$500 \times 500\,\mu$m
L635P5 LD	red laser diode	Thorlabs	∅1.6 mm
HL-2000-FHSA	halogen light source	Ocean Insight	∅3.2 mm

4.2.2 Illumination

For characterization of illumination of LEDs, the following setup was used: the LED was fixed in one position with the lux meter in a fixed distance d_{lux} of 1 cm. The current I_F was set from 0 up to 175, 255 or 750 mA (depending on the LED type). Unless specified, the value of ambient light was 30-40 lx.

In Fig. 4.3, the measured relation between the illumination and the voltage of the LEDs are plotted. Two samples of each of three types of LEDs were

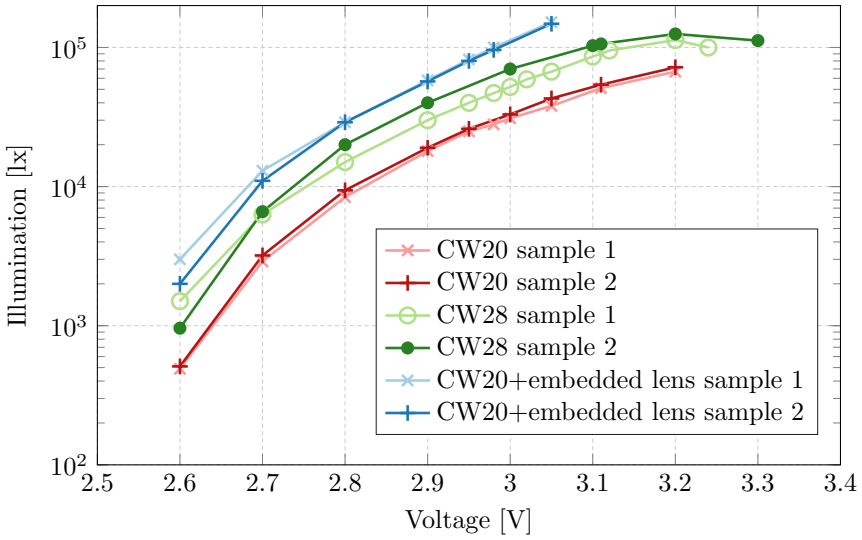

Figure 4.3: Illumination over voltage of two samples of each LED type. The illumination was measured in $d_{\text{lux}} = 1$ cm distance from the LEDs.

measured: 500 × 500 µm LA CW20WP6, 700 × 700 µm LA CW28WP6 and 500 × 500 µm LA CW20WP6 with an embedded lens.

If we compare the LEDs, we can see that by adding a lens over a 500×500 µm LA CW20WP6 LED the illumination performance is increasing, for 3 V the illumination of LED with embedded lens is about 75000 lx higher. But when using the LEDs with a lens I noticed that the LEDs are in fact overheating.This leads to limiting of the range in which the LEDs can be used - when a voltage of more than 3 V was used, the current was increasing, without increasing the illumination level. Because of this overheating, the LEDs with embedded lenses are not used in the final OCC system.

When comparing 500 × 500 µm LA CW20WP6 LEDs with 700 × 700 µm LA CW28WP6 LEDs we can see, that the latter has better illumination performance - for 3 V the illumination of 700 × 700 µm LA CW28WP6 is about 20000 lx higher compared to the 500 × 500 µm LA CW20WP6. Because of this, the 700 × 700 µm LA CW28WP6 LEDs are used in following setups. Note the decrease of illumination after 3.2 V - at this point saturation is reached. This has to be taken into consideration when setting up the LED. Also note that both of the 500 × 500 µm LA CW20WP6 LEDs, with and without the embedded lens, have the same manufacturing properties, the main difference in their illumination performance is caused by the embedded lens.

As mentioned earlier, originally only the 500 × 500 µm LA CW20WP6 LEDs were available, thus the following measurements were carried out with the LED without the embedded lens. See Fig. 4.4 for plot of current over voltage and illumination over voltage for distance d_{lux} of 25 and 50 cm of 500 × 500 µm LA CW20WP6 LED. We can see that when doubling the distance d_{lux} from 25 to 50 cm the illumination of the LED decreased ten times.

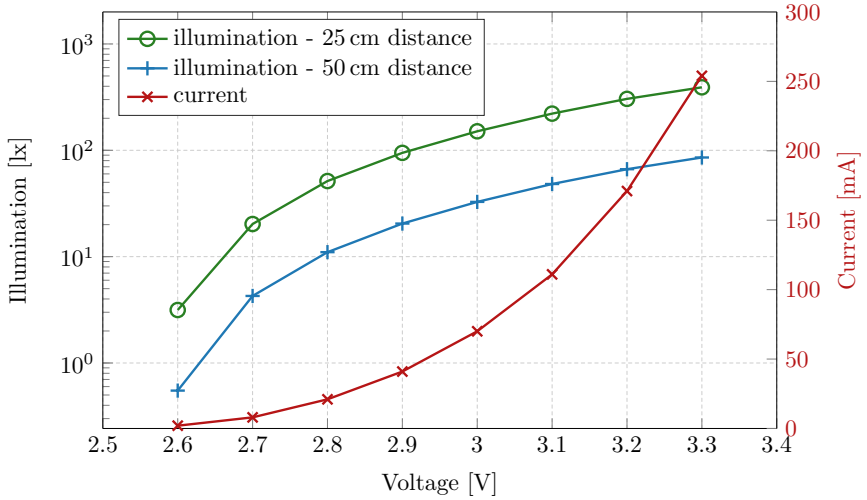

Figure 4.4: Illumination over voltage and V-A characteristics of a 500 × 500 µm LA CW20WP6 LED measured in 25 and 50 cm distance d_{lux} from the LED.

4.2.3 Radiation Pattern

To further characterize the $500 \times 500\,\mu$m LA CW20WP6 LED, the radiation pattern was measured. The LED was attached to the two-axis linear translation stage with rotating platform with the LED in the axis of rotation. Opposite to the LED the lux meter was attached. The optical radiation pattern was obtained in 25 and 50 cm distance. For photo of the measurement configuration, see Fig. 4.5. With the LED, set to $I_F = 300\,$mA and forward

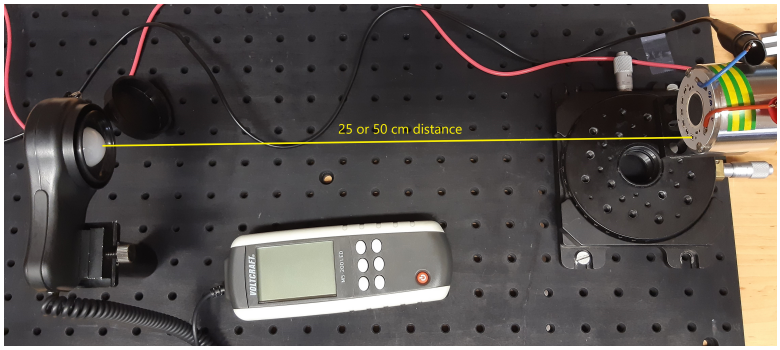

Figure 4.5: Setup for measurement of radiation pattern of LED.

voltage $V_F = 3.3\,$V, was being rotated gradually from -90 to 90° with step of 10°. All measurements of radiation pattern were executed in the far-field.

The measured radiation pattern of the LED for $d_{\text{lux}} = 25$ and 50 cm distances are presented in Fig. 4.6 and Fig. A.4. In the figures the LED is

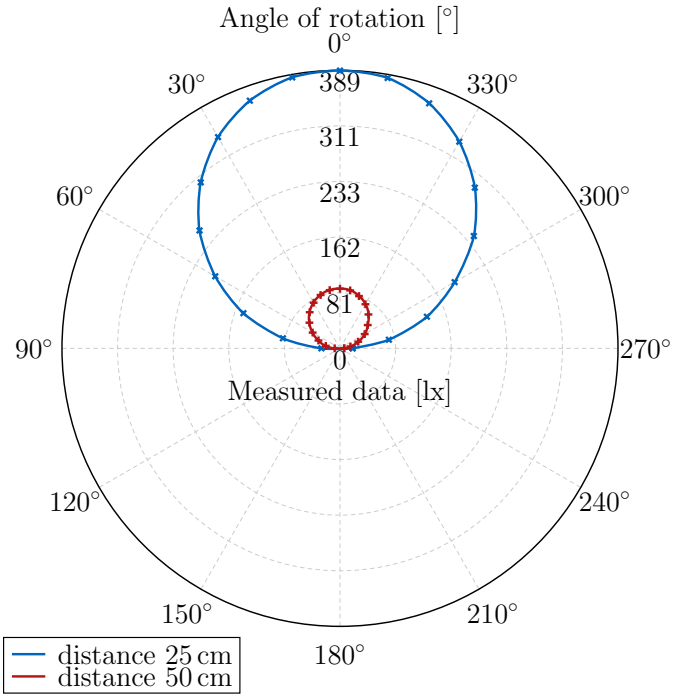

Figure 4.6: Measured radiation pattern of a $500 \times 500\,\mu$m LA CW20WP6 LED for $d_{\text{lux}} = 25$ and 50 cm.

placed in the center of the polar diagram, facing the 0° mark. On the radial axis the illumination is plotted. From the data, we can say that the radiation profile for the LED represents a complete hemisphere and as such is by its shape very close to Lambertian emitter with the order of 1. Fig. A.4 has normalized data to confirm, that the radiation pattern is not changing with distance d_{lux}.

As we can see from the plots, the illumination for distance d_{lux} of 25 cm is, for maximum current, approximately 400 lx. Whereas for $d_{\text{lux}} = 50$ cm and the same current settings, the illumination is about 80 lx, making it about five times lower in the double distance.

4.2.4 Characterization of Light Sources - Conclusion

I analyzed the radiation pattern of the $500 \times 500\,\mu$m LA CW20WP6 LED, being very close to the Lambertian profile. The $700 \times 700\,\mu$m LA CW28WP6 LED is thus expected to have an identical radiation pattern. The difference between $500 \times 500\,\mu$m and $700 \times 700\,\mu$m was mainly in the V-A characteristics. Based on the illumination results, the $700 \times 700\,\mu$m LA CW28WP6 LED was chosen as the most suitable for the following OF-OCC measurements.

4.3 Characterization of IOFs

For my thesis I selected several IOFs. To choose the most suitable one for further OF-OCC application, I needed to characterize them. In this Section the IOF characterization with regards to illumination, radiation pattern, transmission spectrum and color of illuminating light is presented.

4.3.1 List of IOFs

Four types of IOFs were considered - see table 4.3. First, a 1 m-long plastic IOF by Grace (Taiwan) made of PMMA with a 3.6 dB/m attenuation (measured by the cut-back technique, see [22]). The diameters of core and cladding were $d_{\text{core}} = 1.6$ mm and $d_{\text{cladding}} = 2.0$ mm, respectively. Refractive index of core is $n_{\text{core}} = 1.46$.

Table 4.3: List of tested IOFs.

Manufacturer	Fiber type	d_{cladding} [mm]
Grace, Taiwan	PMMA	2.0
ZDEA, China	Super Bright, PMMA	1.5, 2.0, 2.5, 3.0
	Side Glow, PMMA	1.5, 2.0, 2.5, 3.0
Corning Fibrance, USA	"LDF 2", silica	0.9

The second and third types of plastic IOFs were both manufactured by ZDEA company (China) and are both made of PMMA. One type is Super Bright (SB) plastic IOF (the exact names of the IOFs are ZOSS-1.5 to ZOSS-3.0; $n_{\text{core}} = 1.45$) and the other is Side Glow (SG) plastic IOF (with

names ZOS-1.5 to ZOS-3.0; $n_{\text{core}} = 1.55$) and both come in four versions with different outer diameters: $d_{\text{cladding}} = 1.5, 2.0, 2.5$ and $3.0\,\text{mm}$ (thus the names ZOS-1.5, ZOS-2.0 etc.), which have corresponding core diameters: $d_{\text{core}} = 1.2, 1.5, 2.1$ and $2.5\,\text{mm}$. Super Bright IOF is optimized for maximal illumination for shorter section of the fiber (diffusion length (DL) is around $1\,\text{m}$), whereas Side Glow is optimized for maximal length of illumination alongside the fiber (DL is approximately $15\,\text{m}$).

The last IOF was a silica IOF "Corning Fibrance Light-Diffusing Fiber 2" with DL of $1\,\text{m}$ [19]. The diameters of core and cladding were $d_{\text{core}} = 0.17\,\text{mm}$ and $d_{\text{cladding}} = 0.23\,\text{mm}$, respectively. The operating wavelength range is 420 to 700 nm.

4.3.2 Illumination

To monitor the LED-coupling performance, I measured the illumination over the IOF's length. As a light source a $700 \times 700\,\mu\text{m}$ LA CW28WP6 LED was used. The lux meter was placed in $d_{\text{lux}} = 1\,\text{cm}$ distance from the IOF and the illumination over the IOF length was measured with a $10\,\text{cm}$ step. Each IOF was measured twice in the same direction resulting into a plot of decreasing amount of illumination over the IOF's length in which a fitting curve was added. For IOF's illumination measurement the amount of ambient light was minimized.

To determine, whether the inconsistencies in measured data are due to defects in fibers or are created by the nature of the fibers alone, every fiber was measured twice in the same direction (to eliminate the error by changed coupling of light into fiber).

The measured illumination over the length of IOFs is plotted in Fig. 4.7. The result was fitted with an exponential curve. The Super Bright fiber has

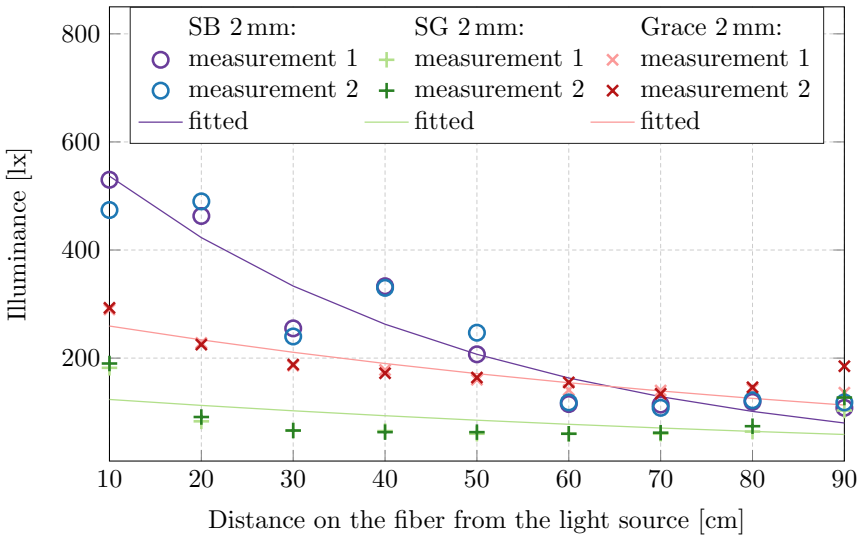

Figure 4.7: Illumination over length of 1 m long section of IOFs. The illumination was measured in $d_{\text{lux}} = 1\,\text{cm}$ distance from the IOFs.

the steepest slope at the beginning of the fiber. This is no surprise, since the very essential feature of the Super Bright IOFs is to a radiate higher percentage of optical power in comparison with other IOFs. And because the Super Bright IOF radiates a higher percentage of its optical power, the amount of power transmitted by this IOF is decreasing more quickly. This leads to an effect noticeable at $50 - 60$ cm in Fig. 4.7 - the illumination of Grace IOF is approximately the same as of Super Bright IOF and beyond this mark the Grace IOF is illuminating more in comparison to the Super Bright IOF. At the beginning of the IOF the Super Bright IOF illuminates about 0.7 and 1.6 times more than the Grace IOF and the Side Glow, respectively. The Side Glow IOF has the flattest slope and at the 50 cm mark the Grace IOF and Super Bright IOF have about 1.7 and 2.7 times higher illumination, respectively.

As we can see in Fig. 4.7, the Super Bright IOF with 2 mm diameter has probably a defect 30 cm from the input. The other two IOFs are defect-free. Note the increase of illumination after 90 cm of fiber. This is most probably caused by reflections at the fiber end facet subsequent power dissipation from the fiber's cladding.

Illumination of Fibrance IOF was measured as well. The illumination is 10 lx at the input of Fibrance, decreasing to 3 lx at Fibrance end. Therefore, the Fibrance was not considered in further measurements with an LED and also its illumination values are not plotted, since the illumination of the plastic IOFs is about 20 to 50 times better.

4.3.3 Radiation Patterns

To examine the radiation pattern of an IOF the Grace IOF was measured with the $500 \times 500\,\mu$m LA CW20WP6 LED as a light source. The IOF was vertically attached into the axis of rotation on a rotational stage with the lux meter placed 2 cm away. The fiber was rotated gradually over 360° a with step of 10° and was measured twice to minimize measurement error. The measurement was performed for 360° rotation to obtain complete information about the spatial illumination distribution around the IOF.

The measured data of the Grace IOF is presented both in original values and in normalized form in Fig. 4.8 and A.5. As we can see from the figures, a slight deviation of $\sim 10\%$ from the maximum normalized intensity appears. This could be caused by small fiber defects, created by fiber bending and stress, or by random inhomogeneity in fiber from production.

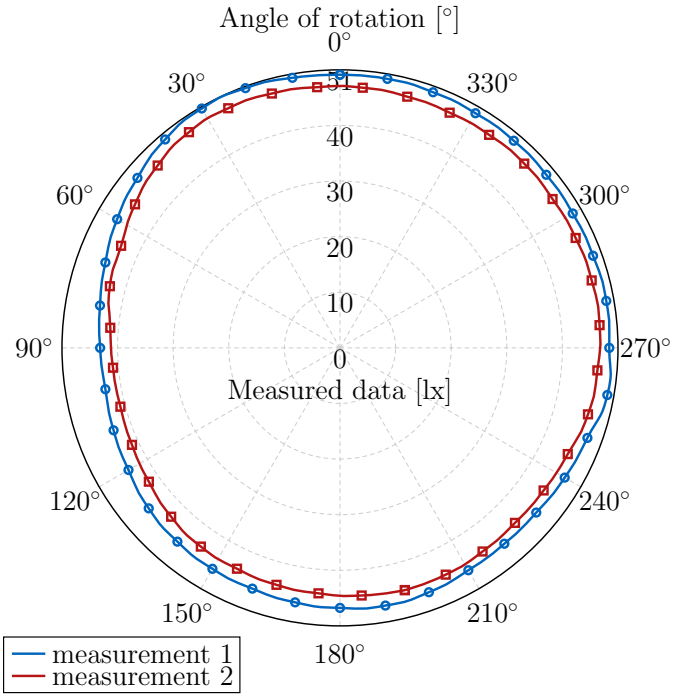

Figure 4.8: Radiation pattern of a 2 mm Grace IOF measured twice in $d_{\text{lux}} = 2\,\text{cm}$ distance.

4.3.4 Transmission Spectra

To understand better the light transmission behaviour of plastic IOFs I measured their transmission spectra. The used setup was a modification of the setup illustrated in Fig. 4.2 - the IOF's end was attached to a 5D stage with the IOF's input as close to the light source as possible, the output of the IOF was attached to an optical spectrum analyser.

The measurements were carried out using the cutback method: for Super Bright and Grace IOF a 2 m long section of fiber was cut to 1 m, for Side Glow a 15 m long section of fiber was cut to 1 m. The transmission of 1 m long section of each fiber was calculated using equation

$$Tx = \frac{10}{l_1 - l_2} \log \frac{P_1}{P_2}, \tag{4.1}$$

where l_1 is the original length of the fiber where the measured spectra are labelled as P_1 and l_2 is the final length of the fiber with measured spectral power P_2.

Complete overview of all measured transmission spectra of plastic IOFs is plotted in Fig. A.6. The selection of the most important measured transmission spectra is depicted in Fig. 4.9. The rest, Fig. 4.10 and Fig. 4.11, shows transmission spectra of Super Bright and Side Glow IOFs, respectively.

Side Glow IOFs (Fig. 4.11) are transmitting a higher amount of power compared to Super Bright fibers. Among Side Glow fibers a decrease in transmitted power in the range $\approx 700 \div 880\,\text{nm}$ is present. That is probably

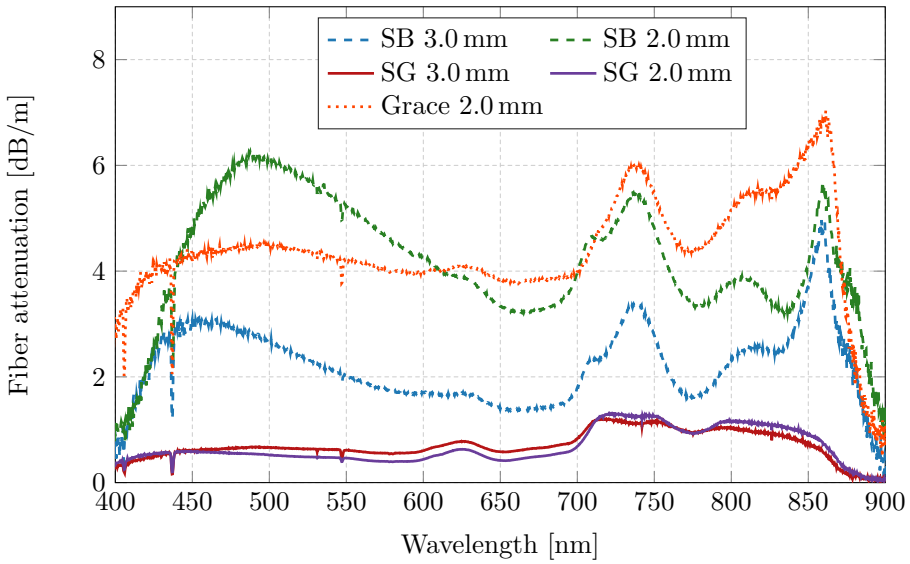

Figure 4.9: Spectral transmission as fiber attenuation of selected IOFs - Super Bright (SB), Side Glow (SG) with various outer diameters (2.0 and 3.0 mm) and Grace IOF.

caused by material absorption of the particular IOFs. Among Super Bright IOFs (Fig. 4.10), the 2.5 mm one has the highest transmission and the 1.5 mm one has the lowest.

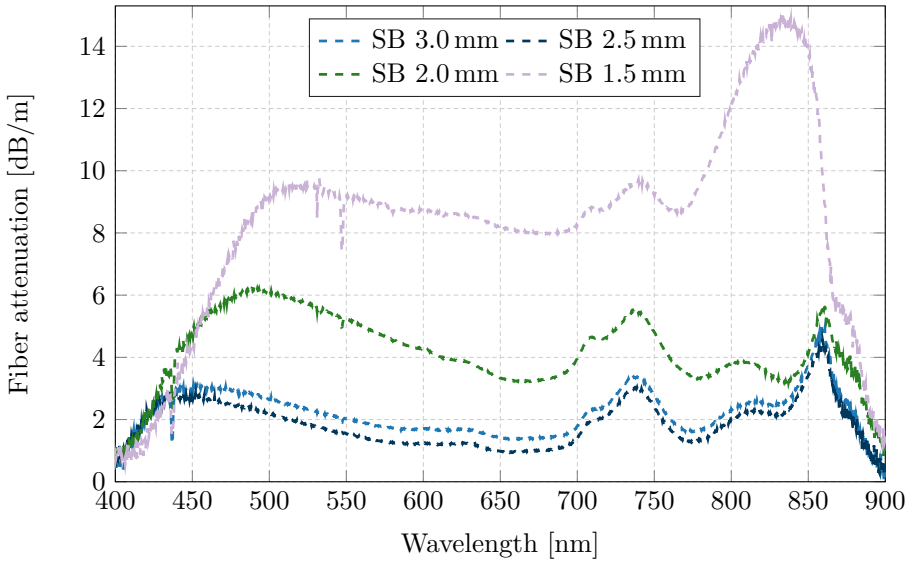

Figure 4.10: Spectral transmission as fiber attenuation of Super Bright IOFs with various outer diameters (1.5 to 3.0 mm).

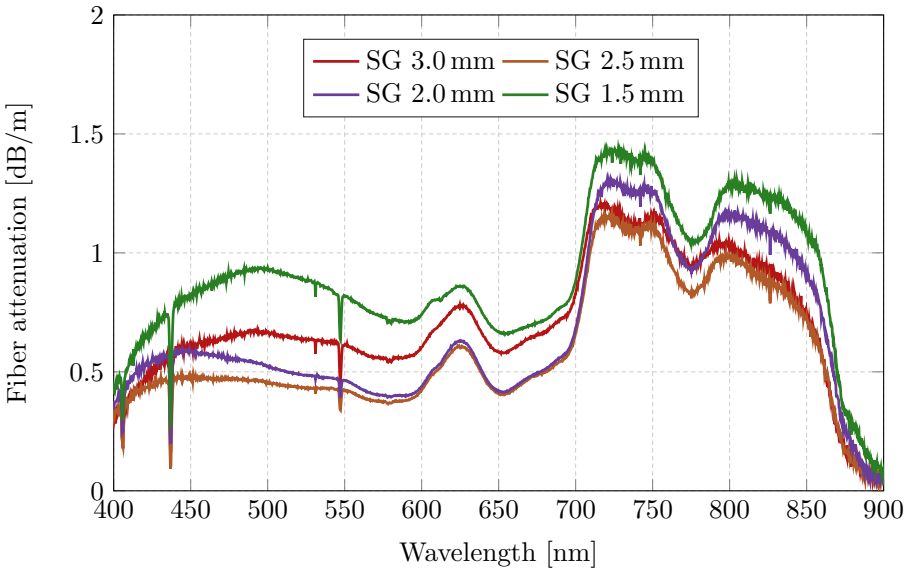

Figure 4.11: Spectral transmission as fiber attenuation of Side Glow IOFs with various outer diameters (1.5 to 3.0 mm).

4.3.5 Change of Color in Plastic IOFs

For application in design and lightning purposes, the radiated spectrum of IOFs is important. In figures 4.12, A.2 and A.3 (some of which are placed in the appendix) all plastic IOFs are compared. For comparison of color a cold white 700 × 700 μm LA CW28WP6 and a warm white 500 × 500 μm LA WW20WP6 LED were used. The light source is placed on the left side of the photographs, light propagates from left to right.

It is apparent that the Super Bright fibers are changing color more dramatically compared to Side Glow fibers. Among Super Bright fibers, the thinner the fiber, the quicker and more pronounced the change of color. See Fig. 4.12a - on the left side of the photograph there is a cold white LED, but after only about 30 cm the color already turns warm white and by the end of 1 m segment of the IOF the color is close to orange. The Side Glow fibers do not change the illuminating color that significantly as Super Bright fibers. For overview of changes of colors in Super Bright IOFs see Tab. 4.4. If the application requires the use of white colored light, the 1.5 mm Super

Table 4.4: Overview of changes of colors in Super Bright IOFs.

Fiber diameter	Color Changes
1.5 mm	beginning CW, 30-60 cm WW, end orange
2.0 mm	beginning CW, at 50 cm turns yellow
2.5 mm	until 90 cm CW, end WW
3.0 mm	after 100 cm turns from CW to WW

Bright IOF is usable only for first 30 cm, the 2.0 mm version could be used in 50 cm long segment, the 2.5 mm Super Bright IOF could be used for 90 cm

(a) : 1.5 mm Super Bright.

(b) : 3.0 mm Super Bright.

Figure 4.12: Colors comparison of Super Bright IOFs with a cold white LED. The light source is placed on the left side, light propagates from left to right.

and if full one meter of IOF is required, from all of the Super Bright IOFs only the 3.0 mm version would be suitable.

These changes of color might be caused by emission of shorter wavelengths (400-500 nm) by a larger magnitude than longer wavelengths (500 nm+). This results into white color turning into yellow or orange at the IOF output. The difference in change of color in Side Glow vs. Super Bright IOFs might be caused by changes in materials, mainly the different refractive index of core (Super Bright: $n_{\text{core}} = 1.45$, Side Glow: $n_{\text{core}} = 1.55$). The Super Bright IOFs are optimized to illuminate on much shorter lengths compared to Side Glow IOFs, where the manufacturer is using a different material composition and these changes lead to different color characteristics.

4.3.6 Characterization of IOFs - Conclusion

Based on the measurement results, the 2.0 mm Grace IOF will not be used in further measurements, since 2.0 mm the Super Bright IOF performs better from the perspective of illumination. The Side Glow IOFs will also not be used in further measurements, since the illumination performance of the 2.0 mm Super Bright IOF is better. The Side Glow IOFs might be convenient in applications where only low illumination but longer IOF segments are needed.

4.4 Optimal Combination for OF-OCC

The optimal combination of a light source and IOF is highly dependent on the intended application. For the purpose of this thesis, lightning application and OCC performance are both sought after. Therefore, plastic IOFs proved to be more suitable as they provide larger fiber diameters compared to silica IOFs. This advantage leads to larger illumination area which is then more easily detectable by the camera.

For the following IOF-based OCC experimental campaign, two combinations of an IOF and a light source were chosen. First, in the pursuit of longer distance OF-OCC system (over 1.5 m) the combination of the 3.0 mm Super Bright fiber with $700 \times 700\,\mu$m LA CW28WP6 LED was selected. Second, for an IOF-OCC system featuring shaped IOF, I have decided for the combination of the 2.0 mm Super Bright with $700 \times 700\,\mu$m LA CW28WP6 LED. The usage of a red LD with the 1.5 mm Super Bright IOF for short distances is also tested.

Chapter 5

OF-OCC Measurements

In the previous chapter I characterized selected IOFs and light sources and based on the results I have chosen their optimal combination of IOF-based OCC which I present in this chapter.

5.1 Proposed Measurements

The experiment setup is the same as in Fig. 4.2. Only the lux meter is now replaced with a camera. In this section fundamental introduction of the measurements properties is presented.

5.1.1 Used Equipment

As mentioned at the end of Section 4.3, the optimal combinations for IOF-OCC are 1 m long section of 3.0 mm Super Bright with $700 \times 700\,\mu$m LA CW28WP6 LED and 0.5 m long section of 2.0 mm Super Bright with $700 \times 700\,\mu$m LA CW28WP6 LED.

Used mechanical components are already listed in the Section 4.2.1. In this measurements, a camera was used as a receiver - industrial camera (IC) capture USB 2.0 (The Imaging Source, DFK 72BUC02) with a resolution of 648×484 pixels and a frame rate $f_R = 25$ fps. The color filter array of this camera is RGB Bayer pattern. Complete overview of devices used in these measurements is in table 5.1.

Table 5.1: An overview of the used devices in the OF-OCC measurements.

Device	Specifications
Camera	The Imaging Source, DFK 72BUC02, USB 2.0 color industrial camera (IC);
Generator	AWG Rohde & Schwarz HMF2550 50 MHz;
DC power supply	GW Instek, GPD-4303S;
Bias-tee	Taylor Microwave, Inc., BT-A11;
LD Controller	Thorlabs, LDC205C 500 mA;
LD Mount	Thorlabs, LDM9T/M.

To generate data, an arbitrary waveform generator (AWG Rohde & Schwarz HMF2550 50 MHz) was used. The signal was sent to the LED via a bias-tee

(Taylor Microwave, Inc., BT-A11) or directly to the LD mount. The LED or LD was attached to the 5D stage (3D micromovement stage Thorlabs, MAX313D/M with pitch and yaw tilt platform Thorlabs, APY002/M).

The camera placement in relation to the IOF is in more details described in the following Sections with specific experiment details and results. Values of the fundamental parameters of the camera are summarised in table 5.2. The used modulation frequency is f_s. Rx camera has given resolution and a frame rate f_R. The exposure time value was set to t_F and gain was G_v. The values listed in this table are an overview of all camera settings used in performed measurements.

Table 5.2: Overview of values of fundamental camera parameters.

Parameter	Value
Rx	IC capture USB 2.0
Resolution	648×484 pixels
f_R	25 fps
t_F	300, 400 & 500 μs
G_v	15, 20 & 30 dB
Data packet size	6 b/packet [010011]

5.1.2 Data generation

When the setup is ready, data transfer can be added. For this experiment a non-return-to-zero (NRZ) on-off-keying (OOK) data format was chosen, since it is the most commonly used data format in OCC. Data packet was created in MATLAB and transferred into the arbitrary waveform generator (AWG). This format of data is then used for intensity modulation (IM) of the LED/LD - the AWG is connected to the bias-tee, which allows to connect both data and DC components to the LED. The LD has its own bias-tee integrated in the LD mount, therefore the AWG is connected directly to the LD mount. The modulated LED/LD is coupling the light into the IOF and the camera is detecting changes in illumination signaling changes of zeros and ones in form of video frames.

In Fig. 5.1 a flowchart of data generation and detection is presented.

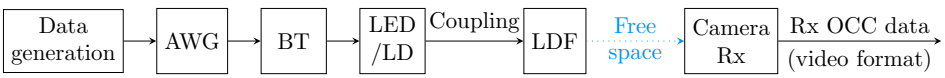

Figure 5.1: Data generation, transfer and detection. The data generated using a computer and an AWG are through bias-tee (BT) brought to an LED/LD. The data in light domain generated by the LED/LD are coupled to an IOF. A camera Rx is detecting the data alongside of the IOF and is capturing it in a video format.

5.1.3 Data processing

The data was captured in form of several video frames, each of which was processed using traditional image processing techniques. The video frames divided into image frames were scanned to locate the captured IOF. From obtained coordinates of the IOF in each image frame a region-of-interest (ROI) is defined. Based on the ROI boundaries a full captured frame is defined and cropped. The cropped ROI image is converted from RGB to gray-scale to retrieve the intensity profile, which is then normalized. Based on the average of the received image intensity profile obtained within the ROI a threshold level is set. To convert the frame into vector, thresholding and binarization of the data frames are performed. At the end of this process transmitted data stream is regenerated and bit steam is calculated. In Fig. 5.2 a flowchart of data processing is presented.

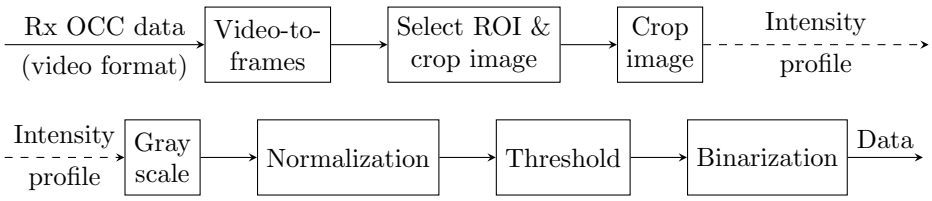

Figure 5.2: Data processing of the video frames captured by the camera.

5.2 Analysis of Illuminating Optical Fiber based Optical Camera Communication System

This Section analyzes the OF-OCC system from the point of view of channel characteristics, bandwidth and data speed limitations and effects of environmental noise (e.g., ambient light) to the system performance. Since the concept of OF-OCC system is novel, as the main sources of information our journal article [22] and conference paper [23] were considered.

Data packets of 6 bits [110010] and [010011], respectively, in non-return-to-zero (NRZ) OOK modulation scheme were generated and transmitted at three modulation frequencies: $f_s = 300$, 500 and 600 Hz. To improve the link performance a repeat packet strategy was used. The published measurements [22], [23] were carried out for following camera settings: exposure time t_F and gain G_v, see table 5.3.

Before the scanned signal is focused on the image sensor (IS), it is amplified while passing through the camera analog-to-digital converter (ADC). This amplification is enhanced according to the software-defined global gain G_v of both the IS and the column amplifier block. The gain G_v is given as

$$G_v = 20 \log_{10} \frac{V_{\text{ADC}}}{V_{\text{pixels}}}, \tag{5.1}$$

Table 5.3: Values of fundamental parameters of published measurements.

Parameter	Value
IOF	2.0 mm Grace IOF
LED's I_F & U_s	300 mA and 3.3 V
Data packet size	6 b/packet
Data sequence	[110010] & [010011]
f_s	300, 500 & 600 Hz
Rx	IC capture USB 2.0
Resolution	648×484 pixels
f_R	25 fps
t_F	200 & 400 μs
G_v	15, 20 & 25 dB

where V_{ADC} is the voltage of the ADC and V_{pixels} is obtained by integration of light during the exposure time as the voltage of a pixel. Therefore, influence of ambient light on the integrity of the data reception can be lessened by higher G_v and lower t_F. Meaning, the signal can be detected even in environment with strong ambient light with higher G_v. The initial proof-of-concept experiments were performed in indoor ambient light conditions.

The measured data is during data processing converted into intensity profiles, which are used to determine 0 and 1 bits as higher and lower intensities in the received image frames and for further thresholding and demodulation. With increasing G_v the intensity profile improves. But to obtain the intensity profile, first the region-of-interest (ROI) must be selected to locate the captured IOF in the image frame and determine the cropping coordinates. The ROI is given [24] by

$$\text{ROI} = \min\left(1, \frac{l_{\text{Tx}} \cdot f_c}{d \cdot l_{\text{IS}}}\right), \tag{5.2}$$

where l_{Tx} is size of the transmitter (Tx), which is in this case created by the IOF, l_{IS} is size of the image sensor (IS) and f_c is the focal length of the camera-based Rx. Using (5.2), the boundaries of the ROI in a full captured frame are defined and the image frame can be cropped using coordinates given as

$$\text{ROI} = \text{Image}[(x_1, y_1); (x_2, y_2)], \tag{5.3}$$

where (x_1, y_1) and (x_2, y_2) are the top-left and bottom-right coordinates, respectively, of the captured IOF in the image frame.

When the ROI is detected, the cropped image is converted from RGB to a gray-scale and the intensity profile is obtained. The intensity profile is further processed using thresholding and binarization, which turns the captured image into the final vector of transmitted data bit stream, which is then decoded. See Fig. 5.2 for schematic of the data processing.

The maximum number of visible bits per group in a single frame is given [25] as

$$N_{\text{visible}} = \lfloor t_{\text{frame}} \cdot f_s \rfloor, \tag{5.4}$$

where f_s is a modulation frequency and t_{frame} is a time frame of the Rx camera and is defined below. The frame time represents amount of time needed to scan one image frame - all of the rows in the rolling shutter camera, and is given [25] as

$$t_{\text{frame}} \leq N_{\text{row}} \times t_{\text{row-shift}} + t_{\text{row-exp}}, \tag{5.5}$$

where N_{row} is the number of pixel rows and is based on the camera resolution, $t_{\text{row-exp}}$ is the exposure time of one row in a frame and $t_{\text{row-shift}}$ is the time delay between the starts of capture of each row in RS capturing mode. In Fig. 5.3 you can see the t_{frame} of a row, including $t_{\text{row-shift}}$ and exposure time of one row $t_{\text{row-exp}}$.

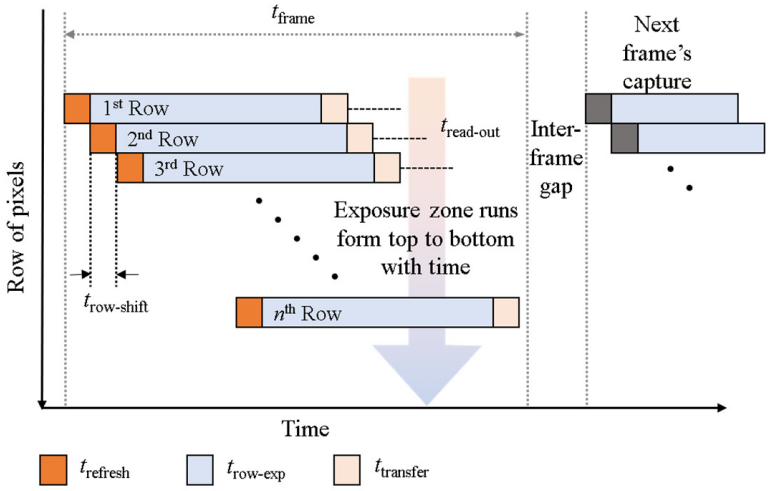

Figure 5.3: Rolling shutter camera capturing mode [25].

Based on N_{visible} the amount of transmitted bits in one frame is given as

$$R_b = N_{\text{groups}} \cdot N_{\text{visible}} \left(\frac{\text{fps}}{2} \right), \tag{5.6}$$

where N_{groups} is the number of groups in a single frame of the data transmission channels in the Tx unit. In OF-OCC system with one IOF and one-channel light source, $N_{\text{groups}} = 1$. For LED array OCC systems with, e.g., 8 rows and 8 columns of LEDs, $N_{\text{groups}} = 8$. Parameter fps represents the camera frame rate, frames per second. The fps value is divided by two to reassure the Nyquist theorem is complied to. Given equations can be combined into

$$R_b = (N_{\text{row}} \times t_{\text{row-shift}} + t_{\text{row-exp}}) \cdot f_s \left(\frac{\text{fps}}{2} \right), \tag{5.7}$$

and the number of transmitted packets R_{packet} is

$$R_{\text{packet}} = \left\lfloor \frac{R_b}{s} \right\rfloor, \tag{5.8}$$

where s is the bit length of one packet in the bit sequence, in this thesis $s = 6$.

Considering that due to camera capture speed limitations only a small number of bits is transmitted, the OCC link performance is analyzed in terms of the reception success. It is defined as the ratio of correctly decoded bits to the total number of transmitted bits. The bandwidth of the transmission link is also limited by used modulation frequency f_s.

In OCC systems in general, received signal $y(t)$ is given by [26]

$$y(t) = \eta G_v x(t) \otimes h(t) + n(t), \tag{5.9}$$

where η is the quantum efficiency of the IS, $x(t)$ is the intensity-modulated light that is being transmitted, $\otimes$ is the time domain convolution, $h(t)$ is the combined impulse response of the channel and the camera and $n(t)$ is the additive white Gaussian noise, including the ambient light induced shot noise and the noise in the camera (i.e., thermal, fixed pattern, photo-current shot and flicker noise sources).

Since the introduced IOF-based Tx has a small surface area for capturing sufficient lights and data bits, the IOF is captured at higher G_v in order to enhance the intensity of captured data. By increasing G_v the influence of ambient light on the integrity of data reception is mitigated.

In the published paper [22], the OF-OCC system performance was as follows: for 50-66 cm camera-fiber distance and $f_s = 300$ Hz success of reception of 97 to 100 % was achieved for t_F of 200 and 400 μs and G_v of 15 and 25 dB, respectively. For the same distance and f_s of 500 Hz the success of reception was >93 % with the same t_F and G_v settings. The success of reception was the better the closer to the LED.

The published experiment results [23] demonstrate that in spite of the 2.0 mm small diameter of the plastic IOF, a flicker-free wireless communications over transmission distances of 50 and 75 cm with modulation frequencies of 300 and 600 Hz. It has been shown that with exposure time 400 μs and gain of 25 dB a 100 % success of reception can be achieved for the camera-based optical Rx.

5.3 OF-OCC Experiments Overview

This Section shows typical captured image frames and corresponding intensity profiles. In table 5.2 is an overview of all used camera settings, values of fundamental parameters are summarised in a separate table for each one of the measurement type. The maximum and minimum distance of Rx from IOF is $d_{\max}$ and $d_{\min}$, respectively. The angle of rotation of Rx is θ, the angle of fiber bend is ψ and corresponding bend radius is R_{IOF}. The LED or LD is powered with current I_F and supply voltage V_s. Used modulation frequency is f_s and modulation voltage is V_{RF}.

In Fig. 5.4 and 5.5 examples of captured image frames with visible ROI and their normalized intensity profiles are shown. Fig. 5.4 is an example of excellent success of reception with negligible number of errors. As can be seen in Fig. 5.4a in ROI each bit is easily distinguishable and in Fig 5.4b there

are no bits near the threshold level equal to one. This example presents a measurement with the LED ($f_s = 300\,\text{Hz}$) and 3.0 mm Super Bright IOF with camera ($G_v = 15, t_F = 300\,\mu\text{s}$) in 100 cm distance from the fiber.

(a) : Image frame - ROI.

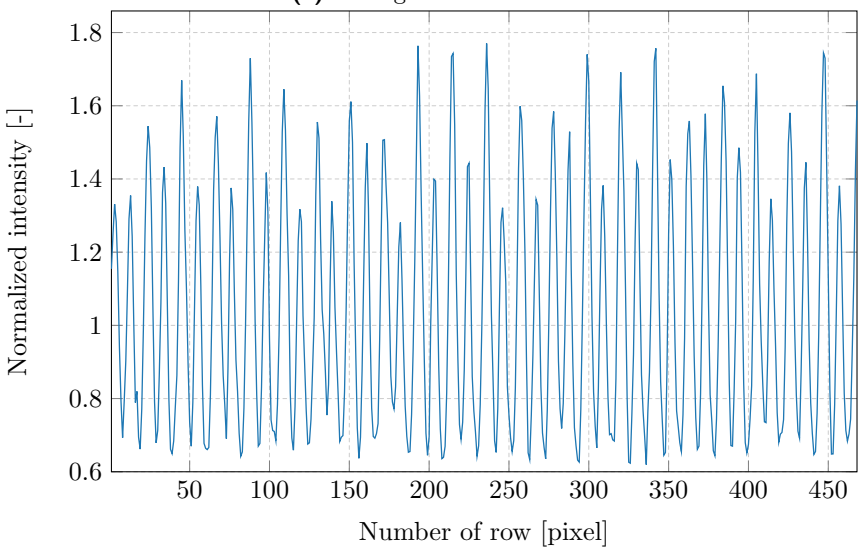

(b) : Normalized intensity profile.

Figure 5.4: Example of captured image frame with visible ROI and its normalized intensity profile:
LED ($f_s = 300\,\text{Hz}$) and 3.0 mm Super Bright IOF with camera ($G_v = 15$, $t_F = 300\,\mu\text{s}$) in 100 cm distance from the fiber, success of reception=98 %.

In Fig. 5.5 an example with the LED ($f_s = 500\,\text{Hz}$) and 3.0 mm Super Bright IOF with camera ($G_v = 20, t_F = 300\,\mu\text{s}$) in 300 cm distance from the fiber is presented. It is indisputable that the first example is giving better results, because in Fig. 5.5b a great deal of bits are much closer to the threshold level compared to previous example. Even ROI is in the first example bigger and better visible than in Fig. 5.5a. Nevertheless, the success of reception is still 73 %, which is a very good result considering the visibility and width of measured ROI.

(a) : Image frame - ROI.

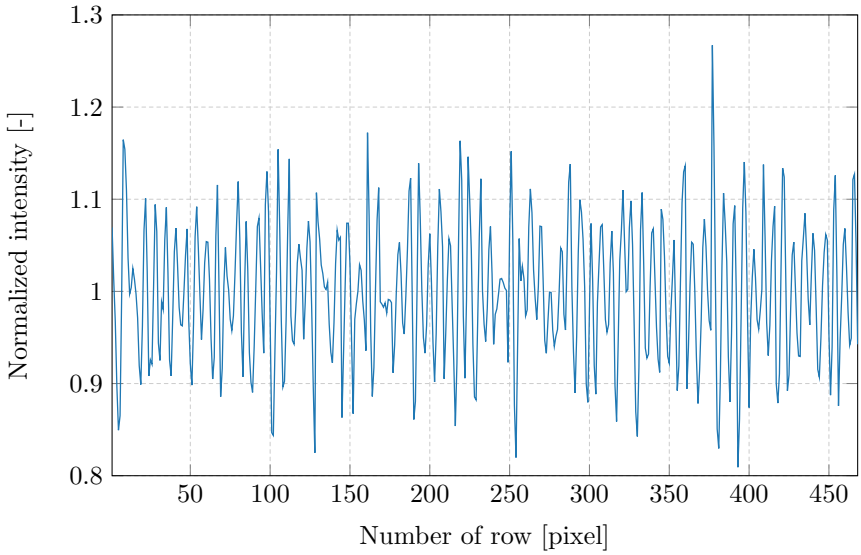

(b) : Normalized intensity profile.

Figure 5.5: Example of captured image frame with visible ROI and its normalized intensity profile:
LED (f_s = 500 Hz) and 3.0 mm Super Bright IOF with camera (G_v = 20, t_F = 300 μs) in 300 cm distance from the fiber, success of reception=73 %.

5.4 Influence of Camera Rotation in Fixed Distance

In the first experiment the Rx camera is placed facing the center of the 1 m long IOF at the distance of 50 cm or 100 cm, as we can see in Fig. 5.6. The Rx is placed on a rotational stage and is rotated (θ) within a $\theta \in \langle -45°; 45° \rangle$ and $\theta \in \langle -27°; 27° \rangle$ interval, respectively. For $\theta = 0°$ the Rx is rotated perpendicular to the IOF and is facing a section of IOF at a 50 cm distance from the light source. This way the camera gradually scans the entire IOF in small intervals of d_f length. The distance of the Rx from the IOF d and size of interval d_f is changing with rotation. As mentioned earlier, maximal d is $d_{\max} = 66$ cm and $d_{\max} = 112$ cm, respectively. Minimal d is $d_{\min} = 50$ cm and $d_{\min} = 100$ cm, respectively.

The measurements with camera rotation were performed to examine the influence of Rx angle position with relation to the IOF. Values of fundamental parameters are listed in table 5.4.

The measured number of error bits is presented in Fig. A.8, and in Fig. 5.7 calculated success of reception is presented. The measured data were fitted with quadratic curve. As you can see from Fig. 5.7, the effect of Rx rotation

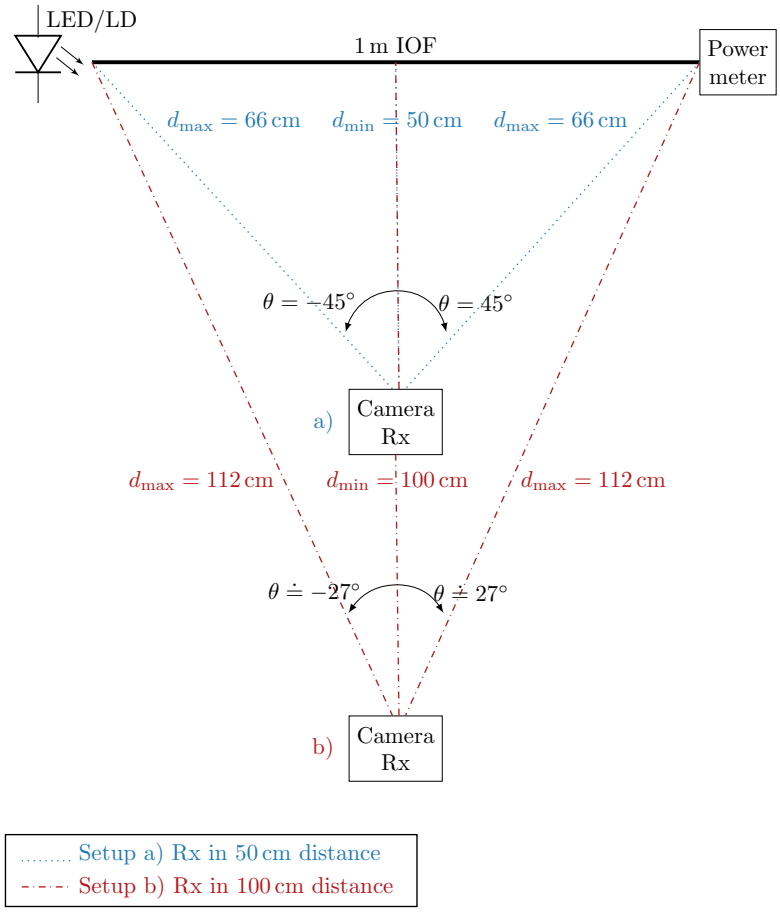

Figure 5.6: Schematic of the IOF-based OCC setup for measurements of influence of camera rotation in fixed distance. The camera Rx was placed in two distances (Setup a) Rx in 50 cm distance, and Setup b) Rx in 100 cm distance). The camera rotation angle θ was changed from -45° up to 45° and from -27° up to 27°, respectively.

Table 5.4: Values of fundamental parameters for measurements with different camera rotation angles.

Parameter	**Value**
IOF	3.0 mm Super Bright
d_{max}	66 & 112 cm
d_{min}	50 & 100 cm
θ	$\langle -45°; 45° \rangle$ & $\theta \in \langle -27°; 27° \rangle$
LED's I_F & V_s	28 mA and 2.8 V
V_{RF}	3.5 V
f_s	300 Hz
t_F	400 μs
G_v	15 dB

is minimal - the overall success of reception is at least 94 % for all angles with less than 3 % deviation. The fitting curve has its maximum for near 0° camera rotation angle for both distances, local minimum for rotation angles

of -45° and -27°, respectively, and global minimum for rotation angles of 45° and 27°, respectively. This means that with the camera facing perpendicularly to the IOF, the success of reception is maximal, and when the camera is being rotated by, the success of reception is the better, the closer to the light source (which is on the left side of the figures, on the IOF at 0 cm distance from the light source). The success of reception has changed by less than 2% with change of camera-IOF distance from 50 to 100 cm.

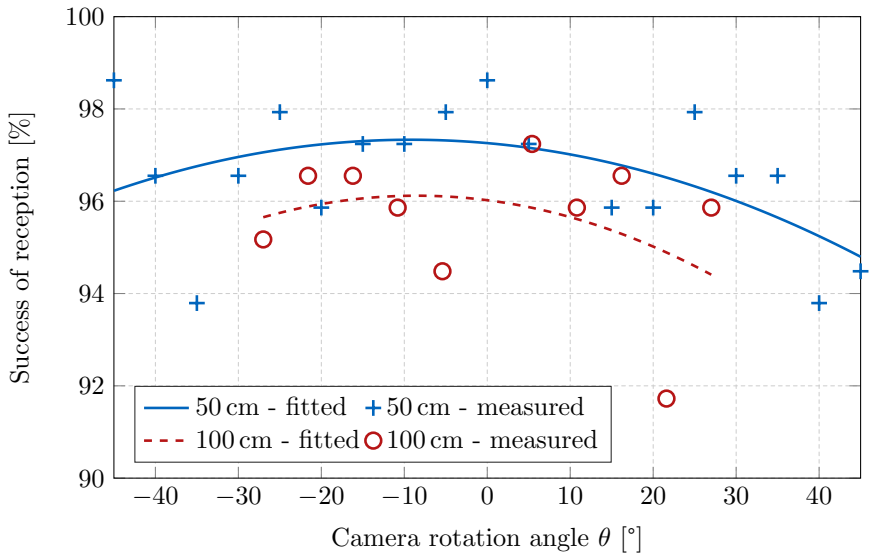

Figure 5.7: Success of reception with different camera rotation angles as illustrated in Fig. 5.6. The camera Rx was placed in the center of the IOF at 50 cm and 100 cm distance. The measured data are fitted by quadratic regression.

5.5 Influences of Different Fiber-Camera Distances and of Changes in Modulation Frequency

In the second experiment, the camera was facing perpendicularly to the IOF at a 50 cm distance from the light source, and the distance of the camera from the fiber was varied from 50 cm up to 300 cm in 25 cm steps.

The measurements with a changing distance of the camera from the IOF and different modulation frequency setting was designed to test the limits of bit transfer for direct fiber-camera view. Values of fundamental parameters are listed in table 5.5. The parameters were optimized for 200 cm camera distance and modulation frequency $f_s = 300$ Hz. With this settings video-frames were captured for distances from 50 cm up to 300 cm and for three modulation frequency values $f_s = 300, 400$ and 500 Hz.

The number of errors in each measurement is plotted in Fig. A.9, and in Fig. 5.8 calculated success of reception is presented. As you can see from the figures, with increasing frequency the number of errors is also increasing and at the same time the success of reception is worsening. The success of

Table 5.5: Values of fundamental parameters for measurements with different fiber-camera distances and with changes in modulation frequency.

Parameter	Value
IOF	3.0 mm Super Bright
$d_{\max}$	300 cm
$d_{\min}$	50 cm
θ	0°
LED's I_F & V_s	28 mA and 2.8 V
V_{RF}	3.5 & 4.0 V
f_s	300, 400 & 500 Hz
t_F	300 & 400 μs
G_v	20 dB

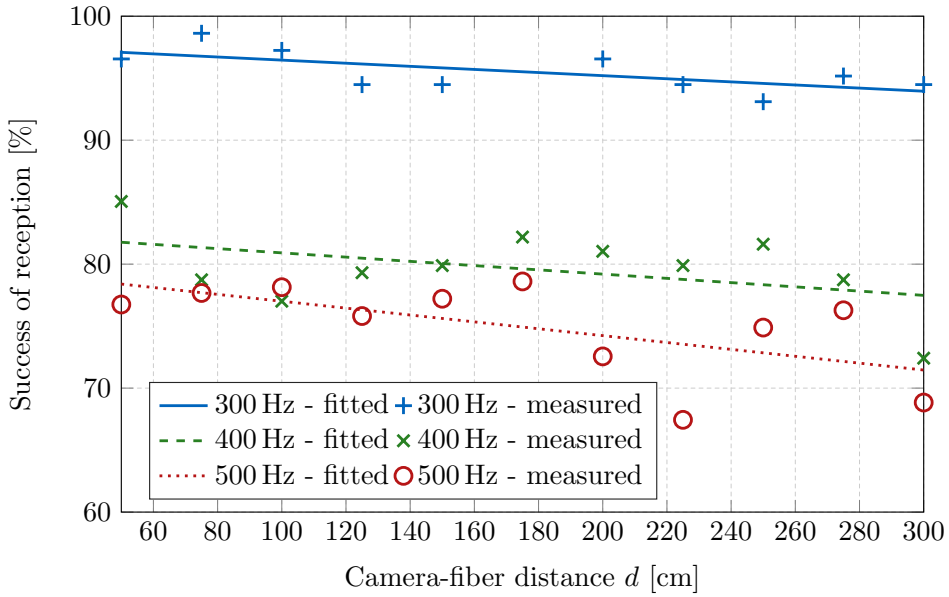

Figure 5.8: Success of reception in measurements with different fiber-camera distances and with modulation frequency of 300, 400 and 500 Hz. The measured data are fitted using linear regression.

reception of 300 Hz is around 95 % for all IOF-camera distances. This values can be considered as extremely high considering the maximum distance of 3 m. The success of reception is increasing as the camera moves closer (from 94 % at 300 cm up to 97 % at 50 cm). The relation between the modulation frequency and the success of reception is in indirect proportionality. For 400 Hz the success of reception is approximately 80 %, which means that the number of errors is around 35 (in comparison - for 300 Hz the number of error bits less than 10), but with increased frequency the total number of transferred bits in one video-frame has increased - from 145 bits up to 175 bits. This means that the number of correctly transferred bits remains effectively the same. The success of reception for 500 Hz is almost as good as for 400 Hz, around 75 %. And again, the number of transmitted bits has increased (up to 215), therefore the loss of 50 to 55 bits leads only to slightly

better performance with lower frequency.

Successes of receptions for all modulation frequencies are fitted using a linear curve. As we can see from Fig. 5.8 for all modulation frequencies, the closer to the IOF, the better the success of reception. Linear fitting curve for 300 and 400 Hz are parallel and the curve for 500 Hz has steeper slope, but it still applies that with increasing distance the success of reception is lowering.

As the number of bits is changing, the number of possible transferred packets is also changing. One packet had 6 bits, meaning that in one video-frame from 22 up to 24 packets can be transferred with modulation frequency of 300 Hz. The total number of transferred packets is not certain because the first and last packet could be accepted incomplete. For modulation frequency 400 Hz the number of possible packets is 27-29 and for 500 Hz it is 33-35 packets.

5.6 Influence of Shaping the IOF

In the third experiment, the IOF was shaped in a defined angle. The coupling from the light source remains fixed, but instead of attaching the IOF in one straight line, 25 cm from the light source a bending mark was placed. Using this mark the fiber was gradually bent from 0 to 90°. The camera was facing perpendicularly to the IOF at a 50 cm distance from both the fiber and the light source, meaning the same section of the IOF at a 25 cm distance after the bend was captured for several different bending angles. The bending angle of the IOF is transformed into radius values. The schematic of this setup is in Fig. 5.9 and photos of the setup are in Fig. A.7.

One of the most interesting advantages of data transfer via IOF is the possibility to bend the fiber into a particular shape. To test whether this idea would be possible in real-life scenarios, the shaped fiber measurement was performed. Values of fundamental parameters are listed in table 5.6.

Table 5.6: Values of fundamental parameters for measurements with different fiber shapes.

Parameter	Value
IOF	2.0 mm Super Bright
$d_{\max} = d_{\min}$	50 cm
θ	0°
R_{IOF}	∞, 81, 58, 45 & 35 mm
ψ	0, 30, 45, 60 & 90°
LED's I_F & V_s	38 mA and 2.8 V
V_{RF}	3.5 V
f_s	300 Hz
t_F	300 μs
G_v	15 dB

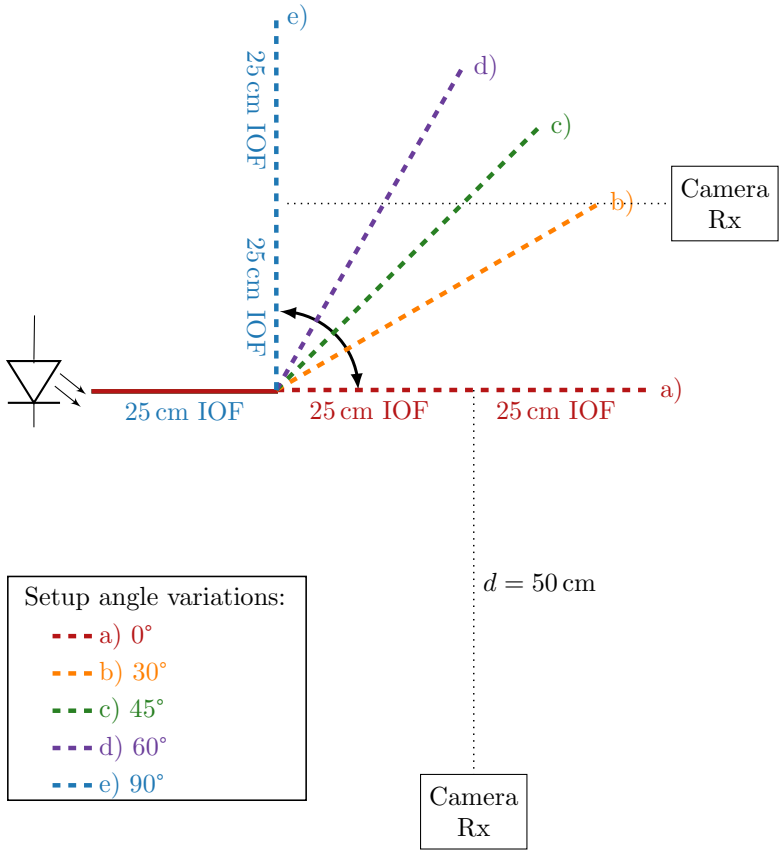

Figure 5.9: Schematic of the setup with IOF shaped in an angle. In 25 cm distance from the light source the IOF was bend. The camera Rx was placed in distance $d = 50$ cm from the IOF facing perpendicularly to a point in 25 cm distance from the bend. The bend was gradually changed from a) 0° up to e) 90°.

The measured values are shown in table 5.7. As you can see from the values, the influence of fiber shape is nearly insignificant. For bending angle of 45° a peak of errors is occurring. This might be caused by measurements errors or it could indicate that bending angle of 45° is the least suitable for shaping of 2.0 mm IOF. But the success of reception is almost perfect for all bending angles, so the effect of the shape of the IOF as presented in this measurement is negligible.

Table 5.7: Values of fundamental parameters for measurements with different fiber shapes.

ψ [°]	R_{IOF} [mm]	Errors [bit]	Success of reception [%]
0	∞	3	98.0
30	81	5	96.6
45	58	7	95.2
60	45	6	95.9
90	35	4	97.2

5.7 Comparison of OF-OCC System with LD and with LED

Examples of video-frames and ROI of IOF with the LED are already shown in Fig. 5.4 and 5.5. In Fig. 5.10 an example of OF-OCC system with the LD ($f_s = 400\,\text{Hz}$) and 1.5 mm Super Bright IOF with camera ($G_v = 30$, $t_F = 400\,\mu\text{s}$) in 50 cm distance from the fiber is presented.

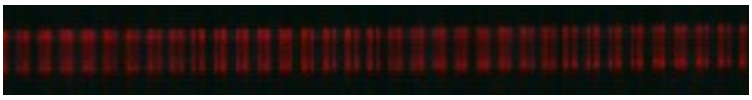

(a) : Image frame - ROI.

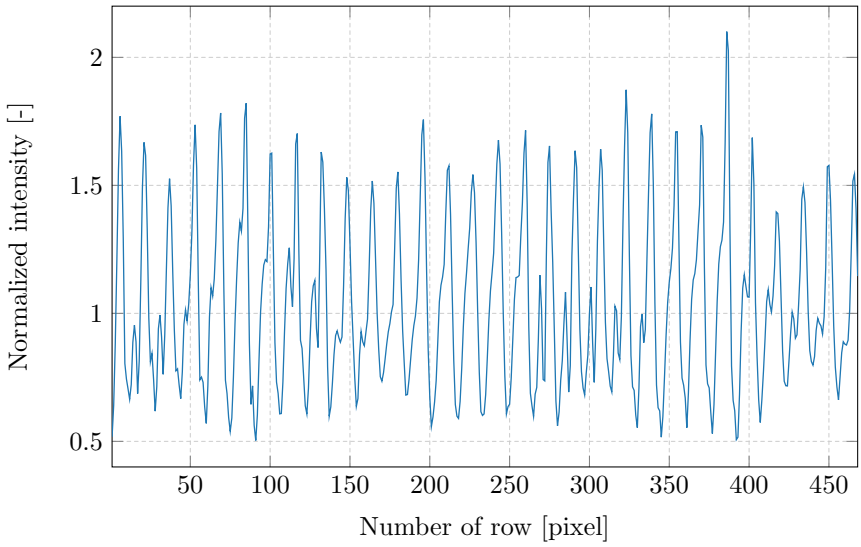

(b) : Normalized intensity profile.

Figure 5.10: Example of captured image frame with visible ROI and its normalized intensity profile:
LD ($f_s = 400\,\text{Hz}$, $V_{\text{RF}} = 3.5\,V$) and 1.5 mm Super Bright IOF with camera ($G_v = 30$, $t_F = 400\,\mu\text{s}$) in 50 cm distance from the fiber, success of reception=71 %.

First noticeable difference is the color of the ROI (Fig. 5.10a) which is in this example red since the LD is using wavelength of 635 nm, but this is insignificant since the ROI is in processing converted to gray-scale. Second difference is the width of the fiber in ROI - in this example a thinner fiber (with diameter of 1.5 mm) was used (in contrast to previous used fiber with diameter of 3.0 mm, Fig. 5.4a and 5.5a). But not only the diameter of the IOF has changed, also the distance of the camera from the fiber - here it is 50 cm, which is two and six time closer in comparison to previous examples. Third, it is clear that the normalized intensity profiles introduced earlier (Fig. 5.4b and 5.5b) with the LED as the light source are much less distorted compared to the measurement with LD - Fig. 5.10b.

The distortion of transmitting bits is visible also in the ROI (Fig. 5.10a).

In some parts of the fiber the bits are spread out less densely and in other parts the fiber is illuminating visibly more. These periodical changes of bits density are taking shape in the illumination profile as well - the maximum value of normalized intensity is periodically increasing and decreasing. This effect might be caused by the fiber itself (1.5 mm Super Bright), but most likely it is due to use of very low frequency with the LD. The assumption is supported by occurrence of the same effect in other types of fiber with the same LD settings.

To compare usefulness of the LD, several measurements with different LD settings were performed. Values of fundamental parameters are listed in table 5.8 and the measured values are shown in table 5.9.

Table 5.8: Values of fundamental parameters for LD vs. LED measurements.

Parameter	**Value**
IOF	1.5 mm Super Bright
$d_{\max} = d_{\min}$	50 cm
θ	0°
LD's I_F	20.2 mA
V_{RF}	3.0 & 3.5 V
f_s	300, 400 & 500 Hz
t_F	400 μs
G_v	30 dB

Table 5.9: Values of fundamental parameters for LD vs. LED measurements.

f_s [Hz]	V_{RF} [V]	Errors [bit]	Success of reception [%]
300	3.5	37	70.9
400	3.0	33	68.6
400	3.5	31	71.3
400	3.5	39	68.3
500	3.5	36	67.0

The number of error bits (as shown in table 5.9) is around 35 bits for each settings variation and the success of reception is again approximately the same - about 70 %. It is obvious that the measured success of reception is not significantly worsened for any of the showed settings options. If we compare these results with previous measurements with the LED and 3.0 mm Super Bright fiber, for $f_s = 300$ the success of reception with the LED and 3.0 mm Super Bright is more than 36 % better than with the LD and 1.5 mm Super Bright for the same distance (96.6 % vs 70.9 %). The difference in the success of reception for other measured modulation frequencies is not that pronounced - the LED values for $f_s = 400$ and 500 Hz for 3.0 mm Super Bright fiber are about 15 and 16 % better than for the same modulation frequencies of the LD and 3.0 mm Super Bright fiber.

To test the effects of a different fiber with LD a 1.5 mm Side Glow IOF was used. However, the measured number of error bits has not changed

significantly in comparison to Super Bright IOF and the distortion effect in the ROI occurred in the measurements with 1.5 mm Side Glow as well.

Chapter 6

Conclusion

The main aim of my thesis was to propose and verify a communication system based on an illuminating optical fiber as a transmitter and an optical camera as a receiver, forming an IOF-based OCC system.

First, I focused on possible light sources from the point of view of radiation patterns and illumination properties. I analyzed three LED types and one laser diode. The $700 \times 700\,\mu$m cold-white LED proved to provide the best performance. Having an embedded lens on the LED grants a more focused radiation pattern. On the other hand; overheating limited the use of maximal illumination, which prohibited reaching better parameters.

Then I characterized selected plastic and silica IOFs. Super Bright, Side Glow, and Grace IOF with outer diameters of 1.5, 2.0, 2.5 and 3.0 mm each were compared. The Super Bright IOFs showed the highest illumination performance at fiber input, with a steeply decreasing slope. After only 50 to 60 cm, the Grace IOF already has higher illumination levels. The illumination of the Side Glow IOF was the most consistent and remained the same for the longest fiber section, and at the same time, its illumination was also the lowest. To further characterize the plastic IOFs, their transmission spectra were measured, and the change of color in Super Bright and Side Glow IOFs was analyzed. The Side Glow IOFs have higher color stability, and among the Super Bright IOFs the thicker the IOF the more stable the color remains.

Based on these measurements, the Super Bright IOFs were chosen for further experiments. The initial measurements showed that the combination of $700 \times 700\,\mu$m LA CW28WP6 LED as a light source, with a 1 m long section of 2.0 and 3.0 mm Super Bright IOF made of PMMA as transmitters is the most promising. The combination of the L635P5 LD by Thorlabs as a light source and 1.5 mm Super Bright IOF was also chosen for further inspection.

I carried out IOF-OCC system measurements in several setup variations. First, the camera Rx was placed in a fixed position and was rotated to analyse the influence of camera rotation on the system performance. For both IOF-camera distances (50 and 100 cm), the success of reception was at least 95 % for all angles.

The second measurement tested the influence of modulation frequency and IOF-camera distance. The camera was facing perpendicularly to the

IOF at a 50 cm distance from the light source, and was moved from 50 cm up to 300 cm in 25 cm steps. For modulation frequency of 300 Hz, the success of reception was more than 94 % even at 300 cm distance. For modulation frequencies of 400 and 500 Hz, success of reception was for all distances around 80 % and higher than 70 %, respectively.

The measurements evaluating the effect of fiber bending showed for all bending angles (0° up to 90°) the success of reception of at least 95 % in 50 cm distance for a modulation frequency of 300 Hz. The measurements with an LD revealed that an LED is for OF-OCC system more suitable as with the LD, the best success of reception was around 70 %.

To conclude, the OF-OCC system performance suggests that for modulation frequency of 300 Hz the system is usable for up to 3 m with 3.0 mm Super Bright IOF, and the success of reception of above 94 % can be achieved.

The proposed OF-OCC system also exhibits meager influence of ambient light on the system performance, and at the same time the success of reception is unchanged by IOF's bending. Therefore, such an OF-OCC system can be used in IoT applications for transmitting simple sensory or identification information.

On the other hand, the proposed OF-OCC system has some limitations, some of which are created by the camera Rx, namely its resolution, lens, and fps. Also, the modulation frequency depends on the synchronization capabilities of the Rx with the Tx.

In my future research, I plan to improve the post-processing algorithm. I aim to study various IOF shapes. Furthermore, with a broader set of acquired data, significant parameters such as mean square error (MSE) or peak signal-to-noise ratio (PSNR) can be calculated. Next, a longer camera-IOF distance can be tested. Moreover, a different light source can be used - e.g., a RGB LED could use two color channels to transmit data and the third color to transmit synchronization information. With this goal, a transfer of more complicated data packets is closely related. Finally, a mathematical model of a full OF-OCC system will be created.

Bibliography

[1] GHASSEMLOOY, Zabih, Pengfei LUO and Stanislav ZVÁNOVEC. Optical Camera Communications. *Optical Wireless Communications: An Emerging Technology.* 1. Switzerland: Springer, [2016]., p. 547-568. Signals and communication technology. ISBN 978-3-319-30200-3.

[2] LIU, Weijie and Zhengyuan XU. Some practical constraints and solutions for optical camera communication. *Philosophical Transactions of the Royal Society A: Mathematical, Physical and Engineering Sciences.* 2020, 378(2169). ISSN 1364-503X doi: 10.1098/rsta.2019.0191.

[3] SKEHILL, Ronan, Padraig SCULLY, Eduardo CANO, Joseph JOHNSON, Sean MCGRATH and John NELSON. Mobility in Wireless Communication Networks. MISRA, Sudip, Subhas Chandra MISRA and Isaac WOUNGANG. I. WORLD SCIENTIFIC, 2010, 2010-04-24, p. 1-41. ISBN 978-981-283-943-5, doi: 10.1142/9789812839442_0001.

[4] ALZENAD, Mohamed, Muhammad Z. SHAKIR, Halim YANIKOMEROGLU and Mohamed-Slim ALOUINI. FSO-Based Vertical Backhaul / Fronthaul Framework for 5G+ Wireless Networks. *IEEE Communications Magazine.* 2018, 56(1), 218-224. ISSN 0163-6804, doi: 10.1109/MCOM.2017.1600735.

[5] GHASSEMLOOY, Zabih, Luis Nero ALVES, Stanislav ZVÁNOVEC and Mohammad-Ali KHALIGHI. *Visible light communications: Theory and Applications.* 1. Taylor & Francis Group, 2017. Electrical Engineering. ISBN 978-1-4987-6754-5.

[6] TURAN, Bugra, Kadir Alpaslan DEMIR, Burak SONER and Sinem Coleri ERGEN. Visible Light Communications in Industrial Internet of Things (IIoT). MAHMOOD, Zaigham, ed. *The Internet of Things in the Industrial Sector.* 1. Cham: Springer International Publishing, 2019, 2019-08-02, p. 163-191. Computer Communications and Networks. ISBN 978-3-030-24891-8, doi: 10.1007/978-3-030-24892-5_8.

[7] LE, Nam Tuan, Mohammad Arif HOSSAIN and Yeong Min JANG. A survey of design and implementation for optical camera communication. In: *Signal Processing: Image Communication.* 2017, p. 95-109. ISSN 09235965, doi: 10.1016/j.image.2017.02.001.

[8] NGUYEN, Trang, Amirul ISLAM, Takaya YAMAZATO and Yeong Min JANG. Technical Issues on IEEE 802.15.7m Image Sensor Communication Standardization. *IEEE Communications Magazine*. 2018, 56(2), 213-218. ISSN 0163-6804, doi: 10.1109/MCOM.2018.1700134.

[9] 7 Technologies: Direct Image Sensor: The Fine Art of Capturing Detail. In: *Sigma DP1x*, 2011. Available from: `http://www.sigma-dp.com/DP1x/technology-colorsensor.html`.

[10] IEEE Standard for Local and Metropolitan Area Networks—Part 15.7: Short-range wireless optical communication using visible light, *IEEE Standard 802.15.7-2011* (2011), doi: 10.1109/IEEESTD.2011.6016195.

[11] LE, Thithanhnhan, Nam-Tuan LE and Yeong Min JANG. OCC-ID: New Broadcasting Service-Based Cloud Model and Image Sensor Communications. *International Journal of Distributed Sensor Networks*. 2016, 12(6). ISSN 1550-1477, doi: 10.1155/2016/1763692.

[12] GUERRA, Victor, Carlos GUERRA, Jose RABADAN, Rafael PEREZ-JIMENEZ and Beatriz ORTEGA. Analysis of Illumination-Fiber-to-Wireless Links. In: *2020 12th International Symposium on Communication Systems, Networks and Digital Signal Processing (CSNDSP)*. IEEE, 2020, 2020-7-20, p. 1-5. ISBN 978-1-7281-6743-5, doi: 10.1109/CSNDSP49049.2020.9249636.

[13] KŘEMENÁKOVÁ, D., J. MILITKÝ, B. MERYOVÁ and V. LÉDL. Characterization of side emitting plastic optical fibers light intensity loss. *World Journal of Engineering*. 2013, 10(3), 223-228. ISSN 1708-5284, doi: 10.1260/1708-5284.10.3.223.

[14] ZAJKOWSKI, Maciej, Ryszard S. ROMANIUK and Krzysztof T. POZNIAK. Emission of flux light in side-light fiber optic. *Photonics Applications in Astronomy, Communications, Industry, and High-Energy Physics Experiments*. 2003, 2003-10-21, 5125, 322-327, doi: 10.1117/12.531531.

[15] LOGUNOV, Stephan, Ed FEWKES, Paul SHUSTACK and Fred WAGNER. Light diffusing optical fiber for Illumination. In: *Renewable Energy and the Environment*. Washington, D.C: OSA, 2013, 2013, DT3E.4-. ISBN 978-1-55752-986-2, doi: 10.1364/SOLED.2013.DT3E.4.

[16] SMITH, Warren J. *Modern Optical Engineering*. 3rd ed. New York: McGraw-Hill, 2000. ISBN 0-07-136360-2.

[17] LANZARINI-LOPES, Mariana, Brandon CRUZ, Sergi GARCIA-SEGURA, Absar ALUM, Morteza ABBASZADEGAN and Paul WESTERHOFF. Nanoparticle and Transparent Polymer Coatings Enable UV-C Side-Emission Optical Fibers for Inactivation of Escherichia coli in Water. *Environmental Science & Technology*. 2019, 53(18), 10880-10887. ISSN 0013-936X, doi: 10.1021/acs.est.9b01958.

[18] LANZARINI-LOPES, Mariana, Zhe ZHAO, François PERREAULT, Sergi GARCIA-SEGURA and Paul WESTERHOFF. Germicidal glow-sticks: Side-emitting optical fibers inhibit Pseudomonas aeruginosa and Escherichia coli on surfaces. *Water Research*. 2020, 184. ISSN 00431354, doi: 10.1016/j.watres.2020.116191.

[19] *Corning Fibrance Light-Diffusing Fiber 2: Specification Sheet*. Corning, 2020. Available from: `https://www.corning.com/media/worldwide/Innovation/documents/Fibrance/Corning_Fibrance_Light_Diffusing_Fiber2_%20FINAL_1.9.20.pdf`.

[20] LEE, Long-Hua and Wen-Chang CHEN. High-Refractive-Index Thin Films Prepared from Trialkoxysilane-Capped Poly(methyl methacrylate)-Titania Materials. *Chemistry of Materials*. 2001, 13(3), 1137-1142. ISSN 0897-4756, doi: 10.1021/cm000937z.

[21] SIDE GLOW FIBER OPTIC. *ZDEA* [online]. Available from: `https://www.pmmafiber.com/side-glow-fiber-optic/`.

[22] TELI, Shivani Rajendra, Klara EOLLOSOVA, Stanislav ZVANOVEC, Zabih GHASSEMLOOY and Matej KOMANEC. Optical camera communications link using an LED-coupled illuminating optical fiber. *Optics Letters*. 2021, 46(11). ISSN 0146-9592, doi: 10.1364/OL.428077.

[23] TELI, Shivani Rajendra, Klara EOLLOSOVA, Stanislav ZVANOVEC, Zabih GHASSEMLOOY and Matej KOMANEC. Experimental Characterization of Fiber Optic Lighting - Optical Camera Communications, *2021 IEEE 32nd Annual International Symposium on Personal, Indoor and Mobile Radio Communications (PIMRC)*, 2021, pp. 1-5, doi: 10.1109/PIMRC50174.2021.9569280.

[24] DUQUE, Alexis, Razvan STANICA, Herve RIVANO and Adrien DESPORTES. Analytical and simulation tools for optical camera communications. *Computer Communications*. 2020, 160, 52-62. ISSN 01403664,doi: 10.1016/j.comcom.2020.05.036.

[25] TELI, Shivani Rajendra, Vicente MATUS, Stanislav ZVANOVEC, Rafael PEREZ-JIMENEZ, Stanislav VITEK and Zabih GHASSEMLOOY. Optical Camera Communications for IoT–Rolling-Shutter Based MIMO Scheme with Grouped LED Array Transmitter. *Sensors*. 2020, 20(12). ISSN 1424-8220, doi: 10.3390/s20123361.

[26] PHAM, Quan, Vega RACHIM, Jinyoung AN a Wan-Young CHUNG. Ambient Light Rejection Using a Novel Average Voltage Tracking in Visible Light Communication System. *Applied Sciences*. 2017, 7(7). ISSN 2076-3417, doi: 10.3390/app7070670.

Appendix A

Figures

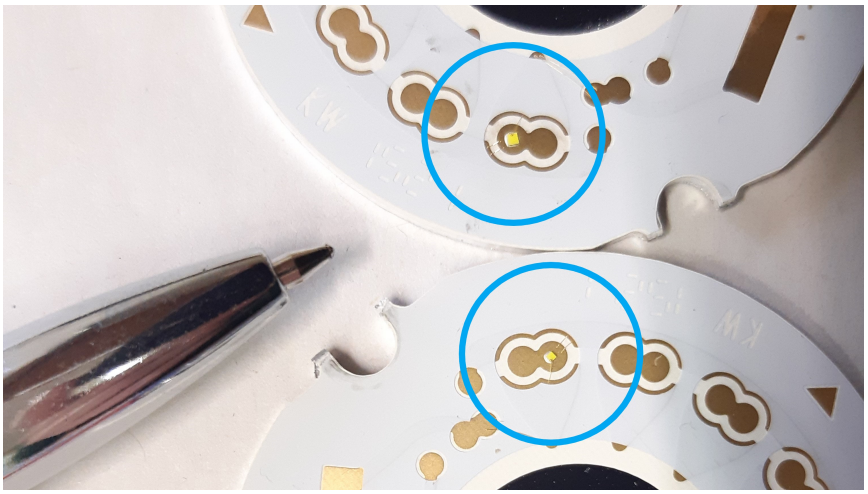

(a) : 700 × 700 μm LA CW28WP6 LED (top) and 500 × 500 μm LA CW20WP6 LED (bottom) with a pen for scale comparison.

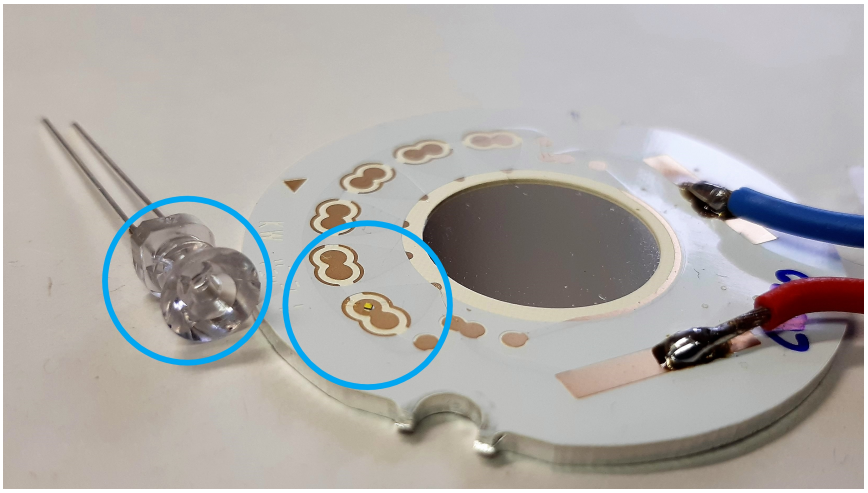

(b) : 500 × 500 μm LA CW20WP6 LED with embedded lens (left) and without (right).

Figure A.1: Photos of the measured LEDs.

(a) : 1.5 mm Super Bright.

(b) : 2.0 mm Super Bright.

(c) : 2.5 mm Super Bright.

(d) : 3.0 mm Super Bright.

Figure A.2: Colors comparison of IOFs with a warm white LED.

(a) : 2.0 mm Super Bright.

(b) : 2.5 mm Super Bright.

(c) : 2.0 mm Side Glow.

(d) : 2.0 mm Grace IOF.

Figure A.3: Colors comparison of IOFs with a cold white LED.

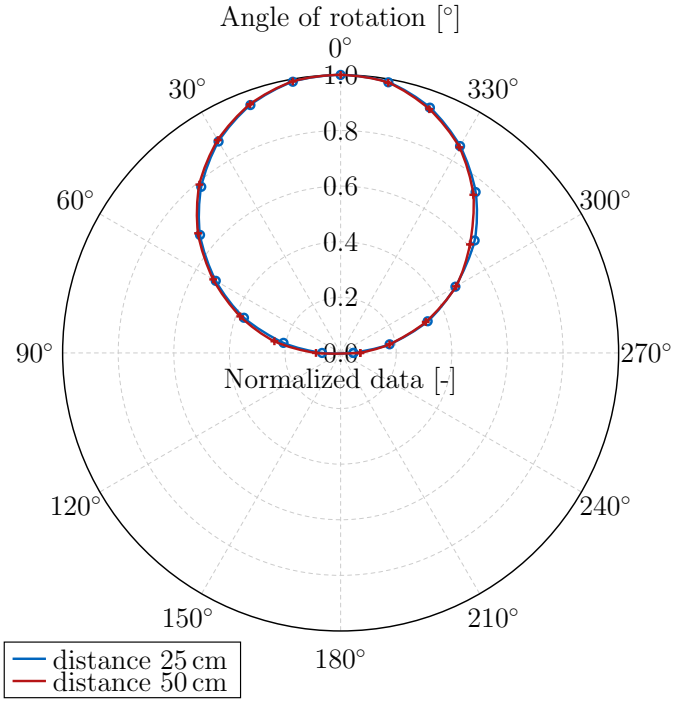

Figure A.4: Normalized radiation pattern of a $500 \times 500\,\mu$m LA CW20WP6 LED for $d_{\text{lux}} = 25$ and 50 cm.

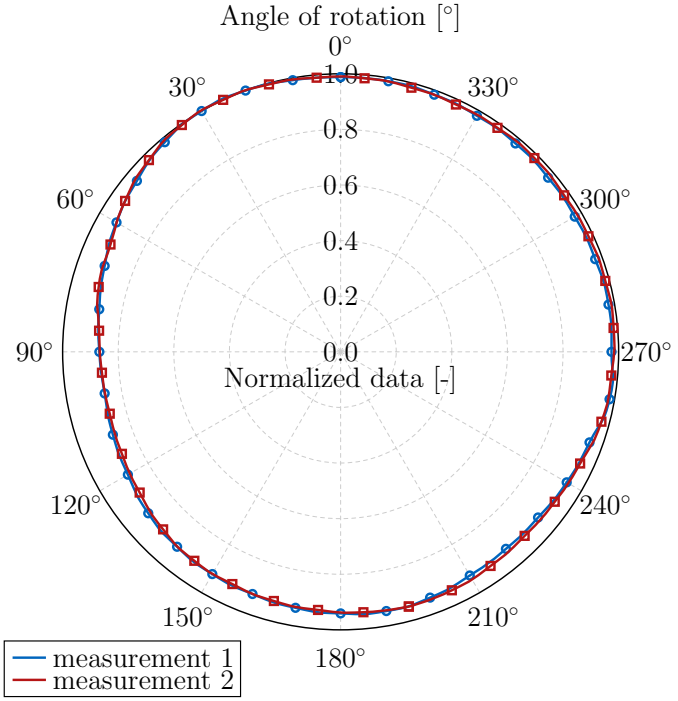

Figure A.5: Normalized radiation pattern of a 2 mm Grace IOF. The IOF was measured twice in $d_{\text{lux}} = 2$ cm distance.

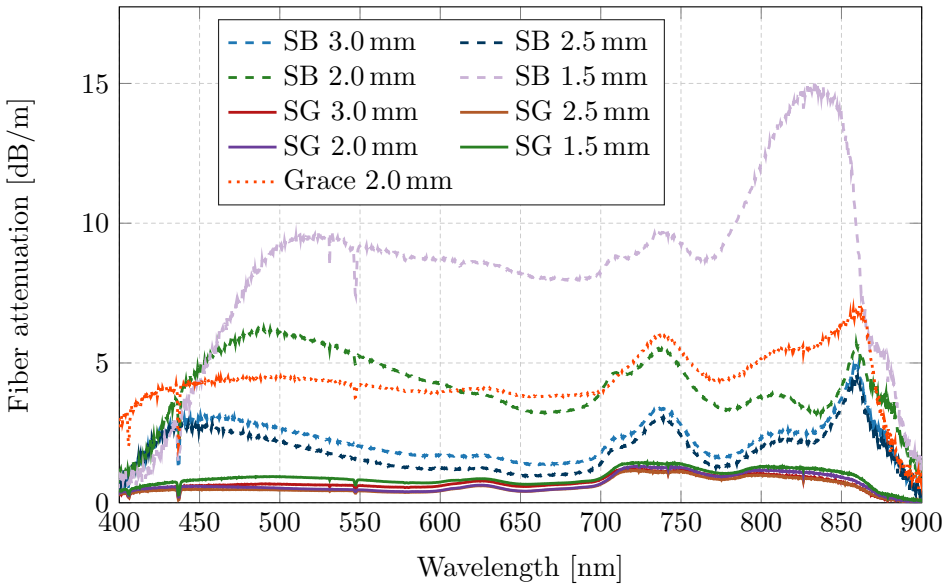

Figure A.6: Spectral transmission as fiber attenuation of all measured IOFs - Super Bright (SB), Side Glow (SG) and Grace IOF with various outer diameters (1.5 to 3.0 mm).

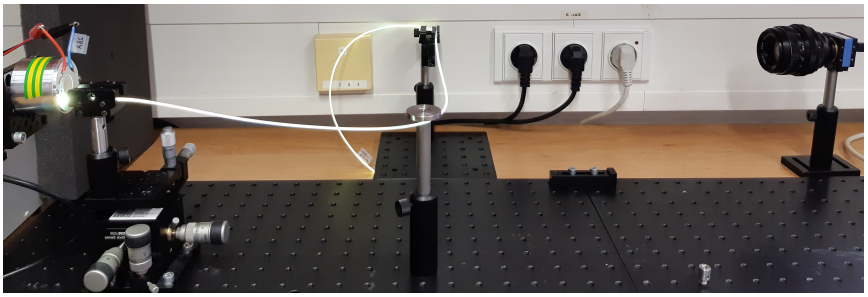

(a) : Side-view.

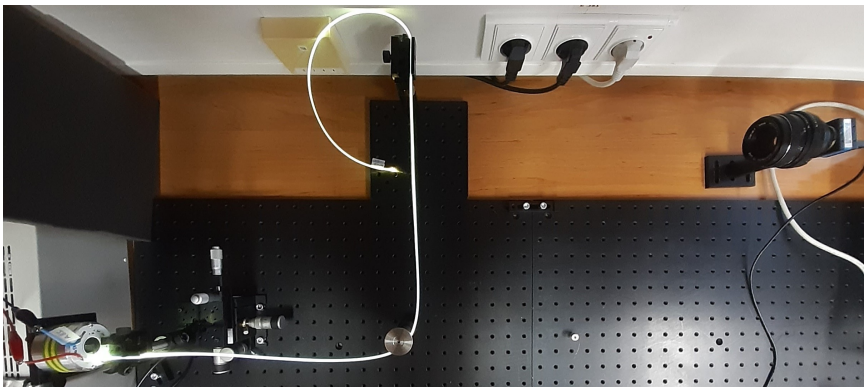

(b) : Top-view.

Figure A.7: Photos of setup of shaped IOF (Super Bright IOF with outer diameter of 2.0 mm) measurements, here for 90° angle. The bend is placed in 25 cm distance from the light source and the camera Rx is facing perpendicularly to a point in 25 cm distance from the bend on the IOF.

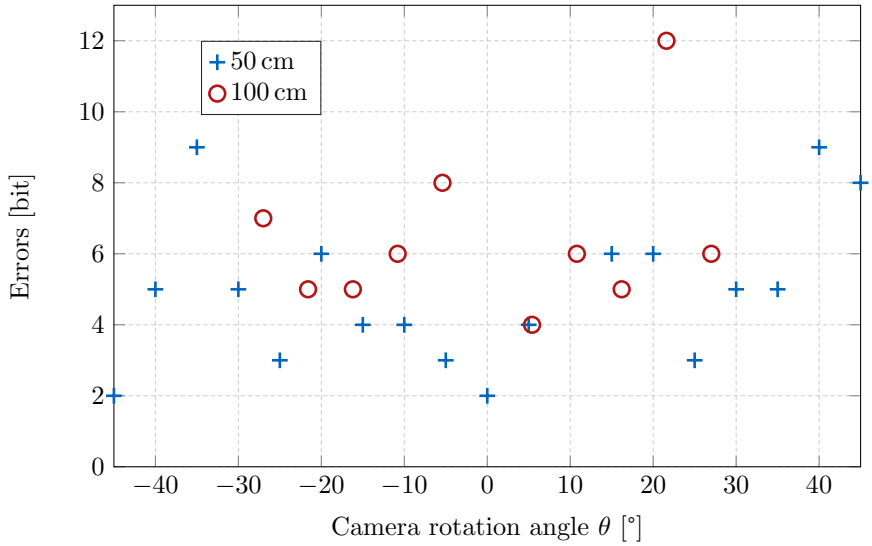

Figure A.8: The number of error bits with different camera rotation angles as illustrated in Fig. 5.6 in the camera-IOF distance of 50 and 100 cm.

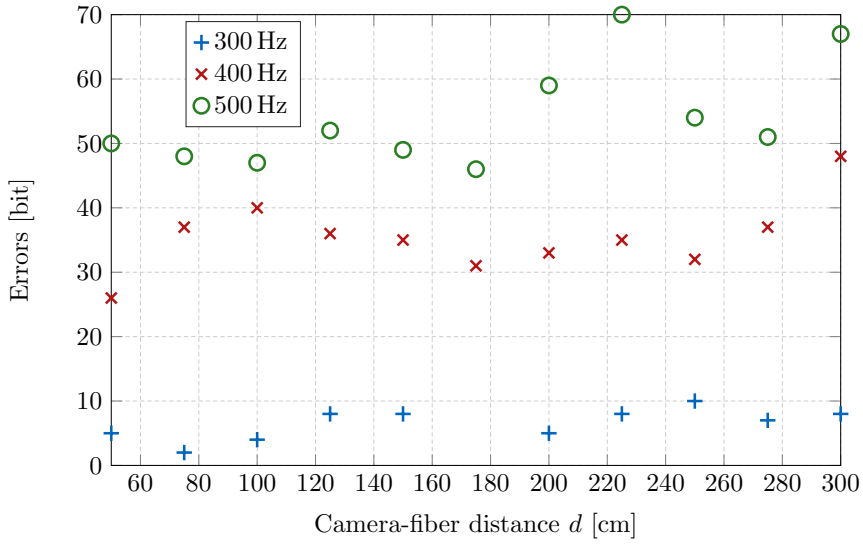

Figure A.9: The number of error bits in measurements with different fiber-camera distances in modulation frequencies of 300, 400 and 500 Hz.